---

**Article:**
Watson, M., Gladwin, D. and Prescott, T. (2021) Collinear mecanum drive: modelling, analysis, partial feedback linearisation, and nonlinear control. IEEE Transactions on Robotics, 37 (2). pp. 642-658. ISSN: 1552-3098

https://doi.org/10.1109/TRO.2020.2977878

---

# The Collinear Mecanum Drive: Modelling, Analysis, Partial Feedback Linearisation, and Nonlinear Control

Matthew T. Watson[1], Daniel T. Gladwin[2], and Tony J. Prescott[3]

***Abstract*—The Collinear Mecanum Drive (CMD) is a novel robot locomotion system, capable of generating omnidirectional motion whilst simultaneously dynamically balancing, achieved using a collinear arrangement of three or more Mecanum wheels. The CMD has a significantly thinner ground footprint than existing omnidirectional locomotion methods, which does not need to be enlarged with increasing robot height as to avoid toppling during acceleration or external disturbance. This combination of omnidirectional manoeuvrability and a thin ground footprint allows for the creation of tall robots that are able to navigate through much narrower gaps between obstacles than existing omnidirectional locomotion methods. This allows for greater manoeuvrability in confined and cluttered environments, such as that encountered in the personal service and automated warehousing robotics sectors.**

**This article derives the kinematics and dynamics models of the CMD, analyses controllability and accessibility, and determines the degree to which a CMD can be linearised by feedback. A partial feedback linearisation is then performed, and three practically useful nonlinear controllers are derived using a backstepping design approach, all with convergence and stability guarantees for the fully-coupled nonlinear model. These are demonstrated both in simulation and on a real-world CMD experimental prototype.**

***Index Terms*—Wheeled Robots, Dynamics, Kinematics, Dynamically Balanced Omnidirectional Motion.**

## I. Introduction

MOBILE robots are seeing increasing deployment in warehousing, retail, and personal robotics applications. Omnidirectional wheel configurations are often used, as these allow for improved mobile manipulation, better navigation of confined and cluttered spaces, and smoother, more graceful motion. Currently, omnidirectional locomotion is typically achieved using three or more omnidirectional wheels, located at the vertices of a polygon beneath the robot. To avoid toppling when accelerating, cornering, or during external disturbance, this ground footprint polygon must be sufficiently large relative to the robot's height. This lower bounds the size of gap between obstacles that can be navigated by robots of a given height, reducing manoeuvrability in confined and cluttered environments and necessitating bulky robot form factors.

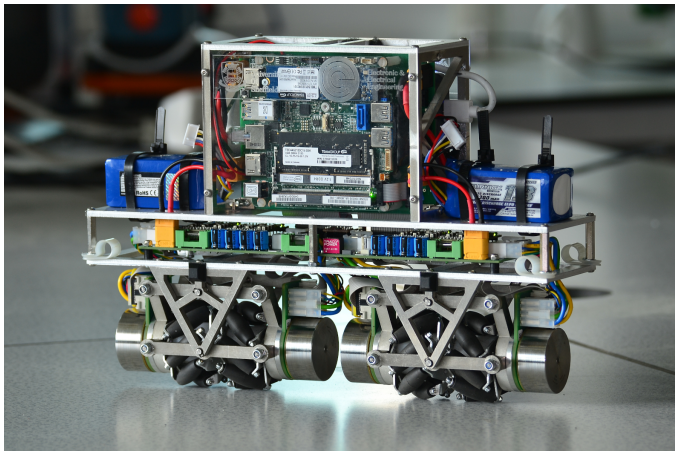

Fig. 1. A Collinear Mecanum Drive prototype, upon which both simulated and experimental results are based.

The Collinear Mecanum Drive (CMD) utilizes three or more collinear Mecanum wheels to enable omnidirectional locomotion whilst simultaneously dynamically balancing about the wheel rotation axis. As the wheels of a CMD are located collinearly, the footprint of a robot using a CMD can be made to be arbitrarily thin, limited only by wheel diameter. As the CMD is omnidirectional, it is able to take advantage of this reduced footprint dimension by translating directly along its wheel axis, allowing for the navigation of smaller gaps between obstacles than existing omnidirectional locomotion methods. This can be achieved whilst maintaining a tall form factor, as stability in this thin dimension is now attained actively rather through possession of a proportionately large footprint. This new locomotion system therefore allows for the creation of omnidirectional systems of the same height as existing statically stable omnidirectional platforms, whilst requiring a fraction of the ground footprint and overall system size, and with a much smaller minimum navigable gap. This enables the creation of tall and slender robots that are better able to navigate cluttered environments such as those encountered in the home, office, and retail robotics sectors.

Omnidirectional dynamically balanced motion has previously only been achieved using either legged or ball-balancing [1] robots. Legged robots are significantly more complex and expensive than the CMD, and do not take advantage of the

*This work was supported by Consequential Robotics Ltd (CqR) and the Engineering and Physical Sciences Research Council [grant number EP/M508135/1]

[1,2]M.T. Watson and D.T. Gladwin are with the Department of Electronic and Electrical Engineering, University of Sheffield, Sheffield, UK. m.t.watson@sheffield.ac.uk, d.gladwin@sheffield.ac.uk

[3]T.J. Prescott is with the Department of Computer Science, University of Sheffield, Sheffield, UK. t.j.prescott@sheffield.ac.uk

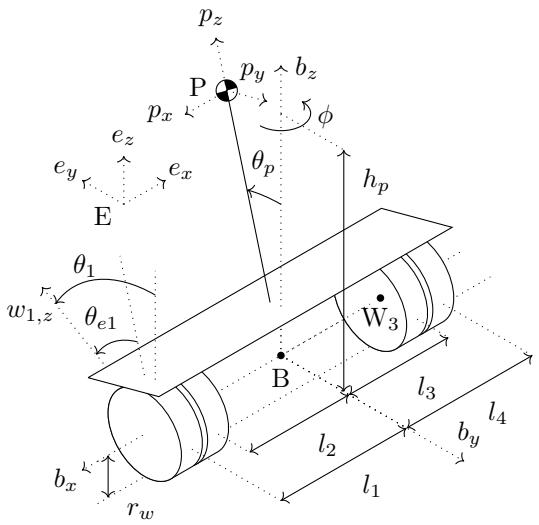


Fig. 2. Collinear Mecanum Drive coordinates and parameters for the experimental prototype shown in Fig. 1

predictable flat terrain typical of indoor environments. Ball-balancing robots are also somewhat complex, are difficult to practically realise, must expend energy to balance in two axes simultaneously, and by possessing only a single ground contact point cannot generate significant torque about the vertical. Comparatively, the CMD requires only three moving parts[1][2], has to balance only in a single dimension, and can generate significant torque about the vertical, allowing for improved control performance and greater environment interaction. The CMD can therefore achieve greater performance than existing omnidirectional dynamically balancing systems, whilst being of simpler construction and likely possessing both greater reliability and reduced unit cost.

Prior to this work only a simple dynamics model of the CMD has been derived [2], and no effort has been made to analyse the controllability or dynamical properties of this novel locomotion system. The CMD has also been shown to be approximately differentially flat [3], allowing for computationally efficient trajectory planning.

## II. Kinematic Model

In order to derive the CMD's inverse kinematics and dynamics models, the nonholonomic constraints imposed by the Mecanum wheels must first be derived.

Consider the proposed CMD platform depicted in Fig. 2 on a flat plane, where $\{\mathrm{E}, \hat{e}_x, \hat{e}_y, \hat{e}_z\}$ denotes the fixed inertial reference frame. The body attached frame $\{\mathrm{B}, \hat{b}_x, \hat{b}_y, \hat{b}_z\}$ is obtained by a rotation of E about $\hat{e_z}$ by $\phi$, followed by a translation of $x\hat{e}_x + y\hat{e}_y$, with B located on the wheel rotation axis in the center of the platform. The pendulum attached frame $\{\mathrm{P}, \hat{p}_x, \hat{p}_y, \hat{p}_z\}$ is obtained by a translation of B by $h_p$ along $\hat{b}_z$, followed by a rotation of $\theta_p$ about $\hat{b}_x$, where $h_p$ represents the height of the pendulum center of mass along $\hat{b}_z$ relative to B, with associated mass $m_p$ and inertia tensor $I_p = \mathtt{diag}(\begin{bmatrix} I_{px} & I_{py} & I_{pz} \end{bmatrix})$. The $i$ wheel coordinate frames $\{W_i, \hat{w}_{i,x}, \hat{w}_{i,y}, \hat{w}_{i,z}\}$ are obtained by a rotation of B about $\hat{b}_x$ by $\theta_i$ and a translation of $\hat{b}_x l_i$, and have identical masses $m_w$ and identical inertia tensors $I_w = \mathtt{diag}(\begin{bmatrix} I_{wx} & I_{wyz} & I_{wyz} \end{bmatrix})$ attached at $W_i$. Only one roller is considered per wheel, and it is assumed to always be positioned directly under the center of the wheel along the $\hat{w}_{i,z}$ axes, with the contact point between this and the ground assumed to be fixed under the center of the roller. This is a simplification, as during rotation of the wheel this contact point actually transitions from one side of the roller to the other, before discontinuously jumping to the start of the next roller as this contacts the ground. Incorporating this phenomena yields a discontinuous model, greatly complicating simulation and model-based control design. The exact contact location is also sensitive to small variations in ground flatness, and is hard to exactly determine in a real-world system. For these reasons this simplification is justified, and is expected to manifest as a cyclic disturbance acting as a torque about $\hat{b}_z$ as each $l_i$ varies over rotation of wheel $i$. The roller axis of rotation $\hat{r}_i$ is defined as a rotation of $\hat{b}_x$ by $\alpha_i$ about $\hat{b}_z$ where $\sin(\alpha_i) \neq 0$ and $\cos(\alpha_i) \neq 0$, with roller angular position given as a rotation about $\hat{r}_i$ by $\Omega_i$. Due to their small size the rollers are assumed to be massless and inertialess for model simplicity.

Considering a single Mecanum wheel, let $\hat{\mu}_p$ represent the unit vector running parallel to $\hat{r}_i$ through the ground contact point, expressed in the local body attached frame, let $W$ represent the wheel's centre, and let the roller contact the ground directly under $W$ at $C$ as $C = W - r_w\hat{b}_z$, where $r_w$ denotes the wheel radius measured to the roller contact point and perpendicular to the wheel rotation axis.

For no slip to occur, the component of the roller's velocity at the contact point along $\hat{\mu}_p$ must always be zero, so

$$\vec{v}_{EC,B} \cdot \hat{\mu}_p = 0 \tag{1}$$

in which $\vec{v}_{EC,B}$ represents the velocity of $C$ relative to E expressed in the local body frame B, and where $\cdot$ denotes the dot product.

$\vec{v}_{EC,B}$ can be expressed as the body frame velocity of the wheel at $W$ relative to E summed with the tangental velocity due to wheel angular velocity $\dot{\theta}_i$ as

$$\vec{v}_{EC,B} = \vec{v}_{EW,B} - r_w\hat{b}_y\dot{\theta}_i \tag{2}$$

Similarly, $\vec{v}_{EW,B}$ can be defined in terms of the body frame velocity of B relative to E as

$$\vec{v}_{EW,B} = \vec{v}_{EB,B} + \dot{\phi}l_i\hat{b}_y \tag{3}$$

Finally, $\vec{v}_{EB,B}$ can be expressed in the inertial frame as

$$\vec{v}_{EB,B} = R_{EB}^T\vec{v}_{EB,E} \tag{4}$$

Combining (1)-(4) and splitting $\vec{v}_{EB,E}$ into its components along $\hat{e}_x$ and $\hat{e}_y$, denoted $x$ and $y$, yields the nonholonomic no-slip constraint

$$\dot{x}\cos(\alpha_i - \phi) - \dot{y}\sin(\alpha_i - \phi) - \dot{\phi}l_i\sin(\alpha_i) + \dot{\theta}_i r_w \sin(\alpha_i) = 0 \tag{5}$$

[1]Excluding the unactuated Mecanum wheel rollers, as compared to a typical moving part within a robot these are very simple and low cost.

[2]Despite requiring only a minimum of three wheels, a four-wheeled configuration is chosen for the prototype in Fig. 1 in order to simplify suspension design.

Similarly, the angular velocity of the roller $\dot{\Omega}_i$ is proportional to its velocity along the vector $\hat{\mu}_t$, where $\hat{\mu}_t$ is perpendicular to $\hat{\mu}_p$ and parallel to the ground, so

$$\vec{v}_{EC} \cdot \hat{\mu}_t = r_r \dot{\Omega}_i \tag{6}$$

which by substitution with (2)-(3) yields the nonholonomic rolling constraint

$$\begin{aligned} \dot{x}\sin(\alpha_i - \phi) + \dot{y}\cos(\alpha_i - \phi) + \dot{\phi} l_i \cos(\alpha_i) \\ - \dot{\theta}_i r_w \cos(\alpha_i) = \dot{\Omega}_i r_r \end{aligned} \tag{7}$$

Equation (5) can be applied to wheels 1 through $n_w$ and rewritten in matrix form to define the platform's inverse kinematic mapping $f^{-1} : (\dot{x}, \dot{y}, \dot{\phi}) \to \dot{\theta}_i$

$$\dot{\theta}_i = \begin{bmatrix} \frac{-\cos(\alpha_i - \phi)}{r_w \sin(\alpha_i)} & \frac{\sin(\alpha_i - \phi)}{r_w \sin(\alpha_i)} & \frac{l_i}{r_w} \end{bmatrix} \begin{bmatrix} \dot{x} \\ \dot{y} \\ \dot{\phi} \end{bmatrix} \tag{8}$$

for $i \in [1 \,..\, n_w]$.

**Remark 1.** *Minimum wheel quantity*

*As the row vector on the left of* (8) *is clearly of rank 1 and dimension 3, a minimum of three wheels, with* $(\alpha_i, l_i)$ *chosen so that the rows of the matrix composed by stacking the row vectors in* (8) *are independent, are required to create a unique forward kinematic mapping* $f : \dot{\theta} \to (\dot{x}, \dot{y}, \dot{\phi})$ *where* $\theta = \begin{bmatrix} \theta_1 & .. & \theta_{n_w} \end{bmatrix}^T$, $n_w \geq 3$.

## III. Dynamics Model

Here the general CMD dynamics model is derived using the Lagrangian method, chosen for its systematic incorporation of nonholonomic constraints. This is derived in terms of generalised positions and local body frame velocities.

There exist two methods of deriving a dynamics model subject to these nonholonomic constraints using the Lagrangian method; Lagrange multipliers can be used to directly incorporate the nonholonomic constraints, or the constraints can be approximately 'holonomised' using the psuedo-inverse of the inverse kinematic transformation matrix. Zimmerman showed both methods to be equivalent in the context of Mecanum wheeled vehicles [4]. Here the former approach is taken.

The system's dynamics equations are derived by use of the Euler-Lagrange equation in terms of generalised coordinates $q$, the Lagrangian $\mathcal{L}(q, \dot{q})$, generalised forces $Q$, Lagrange multipliers $\lambda$, and Pfaffian constraint matrix $A(q)$, defined as

$$\frac{d}{dt}\left(\frac{\partial \mathcal{L}}{\partial \dot{q}}\right) - \frac{\partial \mathcal{L}}{\partial q} = Q + \lambda A(q) \tag{9}$$

where $A(q)$ follows the Pfaffian constraint form $A(q)\dot{q} = 0$.

The generalised coordinates $q$ are selected as

$$q = \begin{bmatrix} x & y & \phi & \theta_p & \theta_1 & \dots & \theta_{n_w} & \Omega_1 & \dots & \Omega_{n_w} \end{bmatrix}^T \tag{10}$$

and from (5) and (7) $A(q)$ is defined as

$$A(q) = \begin{bmatrix} \cos(\alpha_1 - \phi) & -\sin(\alpha_1 - \phi) & -l_1 \sin(\alpha_1) \\ \vdots & \vdots & \vdots \\ \cos(\alpha_{n_w} - \phi) & -\sin(\alpha_{n_w} - \phi) & -l_{n_w} \sin(\alpha_{n_w}) \\ \sin(\alpha_1 - \phi) & \cos(\alpha_1 - \phi) & l_1 \sin(\alpha_1) \\ \vdots & \vdots & \vdots \\ \sin(\alpha_{n_w} - \phi) & \cos(\alpha_{n_w} - \phi) & l_{n_w} \sin(\alpha_{n_w}) \end{bmatrix}$$
$$\begin{bmatrix} 0 & r_w \sin(\alpha_1) & \dots & 0 & 0 & \dots & 0 \\ \vdots & \vdots & \ddots & \vdots & \vdots & \ddots & \vdots \\ 0 & 0 & \dots & r_w \sin(\alpha_{n_w}) & 0 & \dots & 0 \\ 0 & -r_w \cos(\alpha_1) & \dots & 0 & r_r & \dots & 0 \\ \vdots & \vdots & \ddots & \vdots & \vdots & \ddots & \vdots \\ 0 & 0 & \dots & -r_w \cos(\alpha_{n_w}) & 0 & \dots & r_r \end{bmatrix} \tag{11}$$

The Lagrangian $\mathcal{L}(q, \dot{q})$ is found as the difference of kinetic and potential energy in the system $\mathcal{L}(q, \dot{q}) = \mathcal{K}(q, \dot{q}) - \mathcal{U}(q)$, where $\mathcal{K}(q, \dot{q})$ represents the sum of translational and rotational kinetic energy, and $\mathcal{U}(q)$ the total potential energy. The rotational kinetic energy of the system is defined as the sum of rotational energy of the pendulum mass and four wheel masses. As wheel torques act about the $\hat{b}_x$ axis, pendulum inertia $I_p$ must be redefined about $\mathrm{P} - h_p \hat{p}_z$ as $I_{p,b}$, achieved using the parallel axis theorem with translation vector $r_p = \begin{bmatrix} 0 & 0 & -h_p \end{bmatrix}^T$ as

$$I_{p,b} = I_p + m_p \left[ (r_p \cdot r_p) I_{3\times 3} - r_p \otimes r_p \right] \tag{12}$$

where $\otimes$ denotes the outer product. The wheel rotation axes $\hat{w}_{x,i}$ are already aligned with $\tau_i$, so $I_w$ remains unchanged.

This allows rotational kinetic energy $K_r$ to be defined as

$$\mathcal{K}_r(\dot{q}) = \frac{1}{2}\vec{\omega}_p^T I_{p,b} \vec{\omega}_p + \frac{1}{2}\sum_{i=1}^{n_w} \vec{\omega}_{w_i}^T I_w \vec{\omega}_{w_i} \tag{13}$$

where

$$\vec{\omega}_b = \dot{\phi}\hat{b}_z \tag{14}$$
$$\vec{\omega}_p = R_{bp}^T \vec{\omega}_b + \dot{\theta}_p \hat{p}_x \tag{15}$$
$$\vec{\omega}_{w,i} = R_{bw_i}^T \vec{\omega}_b + \dot{\theta}_i \hat{w}_x \tag{16}$$

Similarly, translational kinetic energy is defined as the sum of that of the pendulum and four wheel masses as

$$\mathcal{K}_t(\dot{q}) = \frac{1}{2}\vec{v}_p^T m_p \vec{v}_p + \frac{1}{2} m_w \sum_{i=1}^{n_w} \vec{v}_{w,i}^T \vec{v}_{w,i} \tag{17}$$

where

$$\vec{v}_p = R_{bp}^T R_{eb}^T \begin{bmatrix} \dot{x} & \dot{y} & 0 \end{bmatrix}^T + \vec{\omega}_p \times h\hat{p}_z \tag{18}$$
$$\vec{v}_{w,i} = R_{bw_i}^T R_{eb}^T \begin{bmatrix} \dot{x} & \dot{y} & 0 \end{bmatrix}^T + \vec{\omega}_{w_i} \times l_i \hat{w}_x \tag{19}$$

Finally, potential energy is purely that due to the action of gravity on the pendulum body, defined as

$$\mathcal{U}(q) = m_p g h_p \cos(\theta_p) \tag{20}$$

The generalised forces $Q$ capture all non-conservative forces acting on the system, which here are motor torques $Q_\tau$ and both rolling and viscous friction forces $Q_f$ for $Q = Q_\tau + Q_f$.

The $n_w$ motor drive torques $\tau = \begin{bmatrix}\tau_1 & \dots & \tau_{n_w}\end{bmatrix}^T$ act individually on each wheel, with each also producing an opposing counter-torque on the pendulum body. No motor torques act directly on the $x$, $y$, $\phi$, or $\Omega_i$ generalised coordinates; the interactions between these and the motor torques are instead captured by the nonholonomic constraints (5) and (7). This defines $Q_\tau$ as

$$Q_\tau = \begin{bmatrix} 0_{1\times 3} & \sum_{i=1}^{n_w}(-\tau_i) & \tau^T & 0_{1\times n_w} \end{bmatrix}^T \tag{21}$$

Viscous friction is modelled at two interfaces for this system: at the body-to-wheel revolute joints, with coefficient $k_{vw}$, and at the wheel-to-roller revolute joints, with coefficient $k_{vr}$. It is assumed that $k_{vw}$ is also able to approximate the various motor phenomena that sum to yield a non-zero no-load current. Linear rolling friction is modelled at the roller-to-ground interface as a torque about $\hat{w}_x$ proportional to wheel angular velocity $\dot{\theta}_i$, with coefficient $k_{rw}$. While there will also exist a rolling friction force acting along $\hat{b}_x$, there does not exist a simple experimental approach to allow the independent measurement of this coefficient and $k_{vr}$, so it is assumed that this can be sufficiently captured by the existing $k_{vr}$ coefficient. Tractive friction forces between the roller and ground are already assumed to be infinite in the definition of the nonholonomic constraints in (5) and (7). It is assumed that kinetic friction in the wheel bearings can be fully compensated by application of a discontinuous torque offset to the wheel actuators, allowing its exclusion from the dynamics model, and it is assumed that static friction is negligible for model simplicity. Kinetic friction in the roller bearings cannot be compensated in such a manner, and cannot easily be modelled without introducing a discontinuity, so is therefore treated as a external disturbance. Again, static friction in this interface is also assumed to be negligible for model simplicity.

Viscous friction in the wheel-to-body revolute joint acts proportionally to the difference between each wheel angular velocity $\dot{\theta}_i$ and the pendulum's angular velocity $\dot{\theta}_p$, applying a torque of $k_{vw}(\dot{\theta}_p - \dot{\theta}_i)$ to each $\theta_i$ generalised coordinate and a torque of $\sum_{i=1}^{n_w}(k_{vw}(\dot{\theta}_i - \dot{\theta}_p))$ to the pendulum body $\theta_p$. Viscous friction in the wheel-to-roller revolute joint acts proportionally to $-\dot{\Omega}_i$, applying a torque of $-k_{vr}\dot{\Omega}_i$ to each $\Omega_i$ generalised coordinate. The counter-torque from this friction force acts about two axes on the wheel. That about the $\hat{w}_x$ axis acts to rotate the wheel, applying a torque of $k_{vr}\hat{b}_x \cdot R_{br}\begin{bmatrix}\dot{\Omega}_i & 0 & 0\end{bmatrix}^T$ to each of $\theta_i$. That orthogonal to $\hat{w}_x$ and parallel to the ground imparts an axial load on the wheel, which is transmitted through the wheel mounting to directly apply a force on the pendulum body along the $\hat{b}_x$ axis. This is equivalent to a force acting on the $[x \;\; y]^T$ generalised coordinates of

$$\begin{bmatrix} I_{2\times 2} \\ 0_{1\times 2} \end{bmatrix}^T R_{eb} \begin{bmatrix} \frac{1}{-r_w + r_r} \\ 0 \\ 0 \end{bmatrix} \left( \hat{b}_y \cdot \sum_{i=1}^{n_w} R_{br,i} \begin{bmatrix} k_{vr}\dot{\Omega}_i \\ 0 \\ 0 \end{bmatrix} \right) \tag{22}$$

Rolling friction acting about $b_x$ is proportional to wheel angular velocity $\dot{\theta}_i$.

This defines $Q_f$ as

$$Q_f = \begin{bmatrix} \begin{bmatrix} I_{2\times 2} \\ 0_{1\times 2} \end{bmatrix}^T R_{eb} \begin{bmatrix} \frac{1}{-r_w + r_r} \\ 0 \\ 0 \end{bmatrix} \hat{b}_y \cdot \sum_{i=1}^{n_w} R_{br,i} \begin{bmatrix} k_{vr}\dot{\Omega}_i \\ 0 \\ 0 \end{bmatrix} \\ 0 \\ \sum_{i=1}^{n_w}(k_{vw}(\dot{\theta}_i - \dot{\theta}_p)) \\ -\dot{\theta}_1 k_{rw} + k_{vw}(\theta_p - \dot{\theta}_1) + k_{vr}\hat{b}_x \cdot R_{wr} \begin{bmatrix} \dot{\Omega}_1 \\ 0 \\ 0 \end{bmatrix} \\ \vdots \\ -\dot{\theta}_{n_w} k_{rw} + k_{vw}(\theta_p - \dot{\theta}_{n_w}) + k_{vr}\hat{b}_x \cdot R_{wr} \begin{bmatrix} \dot{\Omega}_{n_w} \\ 0 \\ 0 \end{bmatrix} \\ -k_{vr}\dot{\Omega}_1 \\ \vdots \\ -k_{vr}\dot{\Omega}_{n_w} \end{bmatrix} \tag{23}$$

Introducing $2n_w$ Lagrange multipliers $\lambda = \begin{bmatrix}\lambda_1 & \dots & \lambda_{2n_w}\end{bmatrix}^T$ allows the solution of (9), giving a system of $4 + 2n_w$ ODEs. These can be arranged into the matrix form

$$M(q)\ddot{q} + C(q,\dot{q})\dot{q} + G(q) = A(q)^T\lambda + F(q)\dot{q} + B(q)\tau \tag{24}$$

with symmetric positive semidefinite[3] inertia matrix $M(q)$, Coriolis and centripetal matrix $C(q,\dot{q})$, derived using the Christoffel symbols of $M(q)$ such that $\dot{M}(q) - 2C(q,\dot{q})$ is skew symmetric as

$$c_{i,j} = \frac{1}{2}\sum_{k=1}^{4+2n_w}\left(\frac{\partial M_{ij}(q)}{\partial \dot{q}_k} + \frac{\partial M_{ik}(q)}{\partial \dot{q}_j} + \frac{\partial M_{jk}(q)}{\partial \dot{q}_i}\right)\dot{q}_k \tag{25}$$

and with gravity matrix $G(q)$, viscous and rolling friction matrix $F(q)$, and input matrix $B(q)$.

Provided the conditions set out in Remark 1 are met, examining $\text{rank}(A) = 2n_w$ indicates that $2n_w$ of the model's $4+2n_w$ degrees of freedom are fully constrained by $A$, meaning $2n_w$ generalised coordinates can be made redundant by elimination of the Lagrange multipliers. Defining the nullspace of $A$ as $\Phi$, such that $A\Phi = 0$ and therefore $\Phi^T A^T = 0$, it is evident that $\lambda$ can be eliminated from (24) by pre-multiplication with $\Phi^T$ to yield a reduced dynamic model in terms of the new minimal generalised coordinates vector $p = \begin{bmatrix}x & y & \phi & \theta_p\end{bmatrix}^T$, eliminating wheel and roller angular positions from the dynamic equations.

As the choice of $\Phi$ must satisfy $A^T\dot{q} = 0$, there exists a minimal vector of velocities $v$ that map back to the generalised velocities as $\dot{q} = \Phi v$. As there are infinite solutions for $\Phi$ and therefore choices of $v$, it is possible to choose $\Phi$ such that the rows of $\Phi$ that map $v$ to $(\dot{x}, \dot{y}, \dot{\phi}, \dot{\theta}_p)$ in $\dot{q}$ take the form $\texttt{blkdiag}(R_{EB},\ I_{2\times 2})$, providing a mapping from the

[3] $M(q)$ is usually positive definite in Lagrangian systems, however, in choosing to model the wheel rollers as being massless and inertialess eigenvalues of zero are introduced into $M(q)$.

generalised velocities vector $\dot{q}$ to a more convenient pseudo-velocity vector $v = \begin{bmatrix} v_x & v_y & \dot{\phi} & \dot{\theta}_p \end{bmatrix}^T$ as $v = \Phi^{-1}\dot{q}$.

Premultiplication by $\Phi^T$ and substitution with $\dot{q} = \Phi v$ and $\ddot{q} = \Phi\dot{v} + \dot{\Phi}v$ allows (24) to be rewritten in the reduced generalised coordinates $p$ and pseudo-velocities $v$ as

$$M(p)\dot{v} + C(p,v)v + G(p) = Fv + B\tau \tag{26}$$

in which $M(p)$ is now both symmetric and positive definite, $\dot{M}(p) - 2C(p,v)$ remains skew symmetric, and in which $F$ and $B$ are now invariant in $p$.

As $\det(M(p)) \neq 0 \; \forall \; p \in \mathbb{R}^4$ for sensical parameter choices $M(p)$ is invertible, allowing (26) to be solved for $\dot{v}$ as

$$\dot{v} = M(p)^{-1}(Fv + B\tau - C(p,v)v - G(p)) \tag{27}$$

thus allowing numerical integration of the system dynamics from an initial state $(p_0, v_0)$ with some input trajectory $\tau(t)$.

As $\text{rank}(B) < \dim(\tau)$ when $n_w > 3$, the input $\tau$ may not represent a linearly independent set of inputs. This would mean there exists a linear map $\Lambda : \tau \to u$ that maps $\tau$ onto a minimal simplified set of independent inputs $u$ as $u = \Lambda\tau$, in which there exist infinite choices for $u$. Defining $\hat{B}$ as a basis for the column space of $B$, one suitable map can be found as $\Lambda = \hat{B}^+ B$, where

$$\hat{B} = \begin{bmatrix} 1 & 0 & 0 \\ 0 & 1 & 0 \\ 0 & 0 & 1 \\ 0 & r_w & 0 \end{bmatrix} \quad \Lambda = -\frac{1}{r_w}\begin{bmatrix} \cot\alpha_1 & \dots & \cot\alpha_{n_w} \\ 1 & \dots & 1 \\ l_1 & \dots & l_{n_w} \end{bmatrix}$$

Replacing $B$ in (26) with $\hat{B}$ and using $u = \Lambda\tau$ as the new input yields the new system

$$M(p)\dot{v} + C(p,v)v + G(p) = Fv + \hat{B}u \tag{28}$$

in which $\dim(u) = \text{rank}(\hat{B})$.

Intuitively, the elements of this new input represent force on the body parallel to $\hat{e}_x$, force on the body parallel to $\hat{e}_y$, and torque on the body about $\hat{e}_z$.

A known input $u$ can be mapped back to a choice of $\tau$ in which $\sum_{i=1}^{n_w} \tau_i^2$ is minimised by $\tau = \Lambda^+ u$. If wheel torques are to be constrained this can be enforced by the solution of the constrained least-squares minimisation

$$\min_{\tau} \; \|\tau\|_2^2 \quad s.t. \quad \Lambda\tau = u, \quad |\tau_i| \leq \overline{\tau} \; \forall \; i \in [1 \,..\, n_w] \tag{29}$$

solvable as a quadratic program for feasible choices of $u$ and $\overline{\tau}$.

### A. Controllability

The controllability of a system describes its ability to move from any initial point in its state space $x_0 \in \mathbb{R}^n$ to any other point $x_T \in \mathbb{R}^n$ within finite time $T < \infty$ by manipulation of its inputs $u \in \mathbb{R}^m$. The global controllability of linear systems in the form $\dot{x} = Ax + Bu, \; x \in \mathbb{R}^n, \; u \in \mathbb{R}^m$ is easily proven by determining if the Kalman controllability matrix $C_o$ is of full rank, i.e. $\text{rank}(C_o) = n$, where

$$C_o = \begin{bmatrix} B & AB & \dots & A^{n-1}B \end{bmatrix} \tag{30}$$

Linear systems satisfying this condition can always be globally stabilised to the origin by a feedback of the form $u = -Kx$.

TABLE I
TABLE OF PARAMETERS FOR THE PROTOTYPE IN FIG. 1.

| Parameter | Unit | Value |
|---|---|---|
| $\alpha_1, \alpha_3$ | rad | $\pi/4$ |
| $\alpha_2, \alpha_4$ | rad | $-\pi/4$ |
| $I_{pbx}$ | $\text{kg m}^2$ | 0.0315 |
| $I_{pby}$ | $\text{kg m}^2$ | 0.0534 |
| $I_{pbz}$ | $\text{kg m}^2$ | 0.0271 |
| $I_{wx}$ | $\text{kg m}^2$ | $5.12 \times 10^{-5}$ |
| $I_{wyz}$ | $\text{kg m}^2$ | $1.1 \times 10^{-4}$ |
| $m_p$ | kg | 2.64 |
| $m_w$ | kg | 0.145 |
| $h_{cm}$ | m | 0.072 |
| $h_p$ | m | 0.0874 |
| $-l_1, l_4$ | m | 0.105 |
| $-l_2, l_3$ | m | 0.063 |
| $r_w$ | m | 0.030 |
| $r_r$ | m | 0.0055 |
| $k_{vw}$ | $\text{N m rad}^{-1}\text{ s}$ | $2.3 \times 10^{-5}$ |
| $k_{vr}$ | $\text{N m rad}^{-1}\text{ s}$ | $1.01 \times 10^{-4}$ |
| $k_{rw}$ | N s | $1.97 \times 10^{-4}$ |

Such a proof does not exist for nonlinear systems. A weaker form of this proof is to instead show that a nonlinear system is small-time locally controllable (STLC), and a further weaker form is to show that a nonlinear system is small-time locally accessible (STLA).

Letting $W$ represent an infinitely small region in state space centered around $x_0$, $\mathcal{R}^W$ is defined as the set of configurations $x_T$ that can be achieved by manipulation of $u$ in an infinitely small time $T$ without leaving $W$. A STLC system will be able to use sequences of control input to affect change in $x_0$ in all directions in $W$, meaning $x_0$ will be an interior point within $\mathcal{R}_W$, $p_0 \in \text{int}(\mathcal{R}^W)$, and therefore $\mathcal{R}^W = W$ [5].

A STLA system, whilst still able to locally access a space with the same dimension as $W$, is restricted to accessing a subset $\mathcal{R}_W \subset W$, in which $p_0$ is on the boundary of $\mathcal{R}_W$ and so $p_0 \notin \text{int}(\mathcal{R}^W)$.

**Theorem 1.** *The CMD is STLC from its equilibrium states for sensical model parameters.*

The set of equilibrium states $\mathcal{X}_e$ is defined as the set of states $x$ with constant input $u = 0_{m\times 1}$ at which $\dot{x} = 0_{n\times 1}$, given for the state space $x = \begin{bmatrix} p & v \end{bmatrix}^T$ as

$$\begin{aligned} \mathcal{X}_e &= \{x \mid \dot{x} = f(x,u) = 0, \quad u = 0\} \\ &= \Big\{ \begin{bmatrix} x_1 & x_2 & \dots & x_8 \end{bmatrix}^T \mid (x_1, x_2, x_3) \in \mathbb{R}^3, \\ &\qquad x_4 = \pi k, \quad k \in \mathbb{Z}, \quad x_j = 0, \; j = [5 \,..\, 8] \Big\} \end{aligned} \tag{31}$$

As $0_{n\times 1} \in \mathcal{X}_e$, (28) can be linearised about the stationary upright equilibrium at the origin, yielding a system in the form $\dot{x} = Ax + Bu$, where $A$ and $B$ take the form

$$A = \begin{bmatrix} \begin{bmatrix} 0_{4\times 4} & I_{4\times 4} \end{bmatrix} \\ \begin{bmatrix} 0 & a & 0 & 0 & 0 \\ b & 0 & c & 0 & d \\ 0 & 0 & 0 & e & 0 \\ f & 0 & g & 0 & h \end{bmatrix} \end{bmatrix} \quad B = \begin{bmatrix} 0_{4\times 3} \\ i & 0 & 0 \\ 0 & j & 0 \\ 0 & 0 & k \\ 0 & l & 0 \end{bmatrix} \tag{32}$$

in which $A$ possesses some positive eigenvalues, meaning the upright equilibrium is unstable. Likewise, linearising about any $x \in \{\mathcal{X}_e : x_4 = \pi\}$ yields a negative semidefinite $A$, meaning the lowest pendulum position is a stable equilibrium as expected.

Examining the Kalman controllability rank condition for this system yields $\text{rank}(C_o) = 8 = n$, indicating controllability of the linearised model at the equilibrium states.

A nonlinear system that is controllable when linearised at its equilibrium states is STLC from the equilibrium states for the full nonlinear system [6], meaning the CMD is STLC for $x \in \mathcal{X}_e$ given sensical parameter choices, i.e. $h_p \neq 0$ etc.

For comparison a two-wheeled inverted pendulum moving on a 2D plane yields $\text{rank}(C_o) = 6$, as the nonholonomic constraints imposed by the use of regular wheels prevent translation parallel to the wheel axis. A TWIP on a 2D plane therefore does not satisfy the KCRC, and is therefore not STLC, though a number of authors claim the TWIP to be STLC by analysis of the TWIP's model in joint space [7], which ignores a dimension of the configuration space required to uniquely locate the TWIP on a 2D plane.

**Theorem 2.** *The CMD is STLA* $\forall\ x \in \mathbb{R}^8$.

Arranging (28) in the nonlinear input-affine form

$$\dot{x} = f(x) + \sum_{j=1}^{3} g_j^T(x) u \tag{33}$$

where $x = \begin{bmatrix} p^T & v^T \end{bmatrix}^T$, the drift vector field $f(x)$ and input vector fields $g_j(x)$ take the form

$$f(x) = \begin{bmatrix} x_5\cos(x_3) - x_6\sin(x_3) \\ x_5\sin(x_3) + x_6\cos(x_3) \\ x_7 \\ x_8 \\ f_5(x_4, x_5, x_6, x_7, x_8) \\ f_6(x_4, x_5, x_6, x_7, x_8) \\ f_7(x_4, x_5, x_6, x_7, x_8) \\ f_8(x_4, x_5, x_6, x_7, x_8) \end{bmatrix} \tag{34}$$

$$\begin{bmatrix} g_1^T(x) \\ g_2^T(x) \\ g_3^T(x) \end{bmatrix}^T = \begin{bmatrix} & 0_{4\times 3} & \\ g_{51}(x_4) & 0 & g_{53}(x_4) \\ 0 & g_{62}(x_4) & 0 \\ g_{71}(x_4) & 0 & g_{73}(x_4) \\ 0 & g_{82}(x_4) & 0 \end{bmatrix} \tag{35}$$

in which $g_{53}(x_4) \equiv g_{71}(x_4)$.

The distribution spanned by the vector fields $f$ and $g_j,\ j = [1\ ..\ 3]$ is defined as $\Delta = \text{span}\{f, g_1, g_2, g_3\}$, or in bracket notation $\Delta = \langle f, g_1, g_2, g_3\rangle$, in which $\Delta$ is nonsingular, as assuming sensical parameters $\dim(\Delta) = 4\ \forall\ x \in \mathbb{R}^8$. The accessibility algebra $\mathcal{A}$ is defined as the involutive closure of $\Delta$, written as $\overline{\Delta} = \Delta_{\mathcal{A}}$. A distribution is involutive if $[f, g] \in \Delta\ \forall\ (f, g) \in \Delta$, where $[\ ,\ ]$ denotes the Lie bracket operator, defined as

$$[f_1, f_2](x) = \frac{\partial f_2}{\partial x} f_1(x) - \frac{\partial f_1}{\partial x} f_2(x) \tag{36}$$

The involutive closure of a distribution $\Delta$ can be calculated as the distribution spanned by all possible combinations of Lie brackets calculable from its vector fields, which can be derived iteratively as

$$\Delta_1 = \Delta, \quad \Delta_i = \big\langle \big\{ \Delta_{i-1}, \{[X, Y] \mid X \in \Delta_1, Y \in \Delta_{i-1}\} \big\} \big\rangle, \quad i \geq 2 \tag{37}$$

This procedure terminates when $\Delta_{i+1} = \Delta_i = \Delta_{\mathcal{A}}$, with the terminal value of $i$ required to define this distribution referred to as the nonholonomy degree of the system, with an upper bound of $i \leq n - m$ [8].

For the system (33), clearly $\dim(\Delta_1) = 4$. $\Delta_2$ is calculable as

$$\Delta_2 = \langle \{\Delta_1,\ [\Delta_1, \Delta_1]\} \rangle \tag{38}$$

which in knowing $[f, f] = 0$, $[G, G] = 0\ \forall\ g_j \in G$, where $G = \{g_1, g_2, g_3\}$, can be simplified to

$$\begin{aligned} \Delta_2 &= \langle \{\Delta_1,\ [f, G]\} \rangle \\ &= \langle \{f, g_1, g_2, g_3, [f, g_1], [f, g_2], [f, g_3]\} \rangle \end{aligned} \tag{39}$$

yielding $\dim(\Delta_2) = 7$. $\Delta_3$ is calculable as

$$\Delta_3 = \langle \{\Delta_2,\ [\Delta_1, \Delta_2]\} \rangle \tag{40}$$

in which a single additional Lie bracket is required to yield the distribution

$$\mathcal{D} = \langle \{f, g_1, g_2, g_3, [f, g_1], [f, g_2], [f, g_3], [f, [f, g_1]]\} \rangle \tag{41}$$

that is of full rank $\dim(\mathcal{D}) = n$, meaning $\mathcal{D} = \overline{\mathcal{D}}$, and therefore $\Delta_3 \equiv \mathcal{D} \equiv \Delta_{\mathcal{A}}$. This indicates a nonholonomy degree of 3, the same as a TWIP [9], [10]. Unlike a TWIP, it is found that $\dim(\Delta_3) = n$ even for the frictionless $h_p = 0$ case, indicating STLA even when the pendulum mass generates no force on the body due to gravity. This is intuitive, as the full Cartesian state space can be accessed by combinations of rotation about $\hat{b}_z$ and translation along $\hat{b}_x$, whilst using the rotational dynamics about $\hat{b}_x$ to purely control the $\theta_p$ subsystem. As $\dim(\Delta_{\mathcal{A}}) = n$ this proves that the CMD is STLA $\forall\ x \in \mathbb{R}^n$.

**Theorem 3.** *The CMD is kinematically holonomic*

*The kinematic model of a CMD can be expressed as a sum of vector fields in the form*

$$\dot{p} = \Psi v = \sum_{j=1}^{4} g_j^T(p) v \tag{42}$$

*As the accessibility distribution formed by these vector fields* $\Delta_{\mathcal{A}} = \langle \overline{\Psi} \rangle$ *is found to have full rank* $\dim(\Delta_{\mathcal{A}}) = \dim(p)$*, the individually nonholonomic constraints* (5) *and* (7) *are together completely integrable, meaning as in conventional statically stable Mecanum wheeled vehicles the kinematic model of the CMD is holonomic [8].*

### *B. The Largest Feedback Linearisable Subsystem*

Using the adjoint representation of the Lie bracket $[f, g] = \text{ad}_f g$, successive Lie brackets of the vector fields $f$ and $g$ up to $j$ iterations can be defined as

$$\text{ad}_f^j g = \text{ad}_f(\text{ad}_f^{j-1} g), \quad e.g. \quad \text{ad}_f^2 g = [f, [f, g]] \tag{43}$$

Following the notation of [11]

$$\begin{aligned} G &= \{g_1, g_2, g_3\} \\ G_f &= f + G = \{f + g : g \in G\} \\ \mathrm{ad}_f^j \Delta &= \left\{ \mathrm{ad}_f^j X : X \in \Delta \right\} \\ [\Delta_1, \Delta_2] &= \{[X, Y] : X \in \Delta_1, Y \in \Delta_2\} \end{aligned} \tag{44}$$

define the distributions

$$Q_0 = \langle g_1, g_2, g_3 \rangle, \quad Q_i = \left\langle \left\{ \overline{Q}_{i-1},\ \mathrm{ad}_f^i Q_0 \right\} \right\rangle \quad i \geq 1 \tag{45}$$

where $\overline{Q}_i$ denotes the involutive closure of $Q_i$.

Again, it is clear from the structure of (35) that $\{[g_1, g_2], [g_1, g_3], [g_2, g_3]\} = 0$, so $Q_0$ is involutive and therefore $Q_0 = \overline{Q}_0$. $Q_1$ is calculated as

$$\begin{aligned} Q_1 &= \left\langle \left\{ \overline{Q}_0,\ \mathrm{ad}_f Q_0 \right\} \right\rangle \\ &= \langle \{g_1, g_2, g_3, [f, g_1], [f, g_2], [f, g_3]\} \rangle \end{aligned} \tag{46}$$

with involutive closure

$$\begin{aligned} \overline{Q}_1 = \langle \{ & g_1, g_2, g_3, [f, g_1], [f, g_2], [f, g_3], \\ & [g_1, [f, g_1]], [[f, g_1], [f, g_3]] \} \rangle \end{aligned} \tag{47}$$

which is found to be of full rank $\dim(\overline{Q}_1) = n$, meaning $Q_2$ must be equivalent as $Q_2 \equiv \overline{Q}_1$.

From these distributions the following sequence of nonincreasing integers are computed [11], [12]

$$r_0 = \dim(Q_0) \tag{48}$$

$$r_i = \dim(Q_i) - \dim(\overline{Q}_{i-1}), \quad i \geq 1 \tag{49}$$

$$k_i^* = \mathrm{card}\{r_j \geq i \mid j \geq 0\} \tag{50}$$

in which it is found $r_0 = 3,\ r_1 = 6 - 3 = 3,\ r_2 = 8 - 8 = 0$, giving controllability indices $k_1^* = 2,\ k_2^* = 2,\ k_3^* = 2,\ k_4^* = 0$. This indicates that the largest feedback linearisable subsystem has dimension $n_\lambda = k_1^* + k_2^* + k_3^* = 6$ [11], meaning this subsystem can be rewritten as three linear double integrators. Intuitively, this subsystem will encompass the $(\phi, \dot{\phi})$, $(\theta_p, \dot{\theta}_p)$, and $(\int v_x, v_x)$ dynamics, with the $(\int v_y, v_y)$ dynamics therefore not linearisable by static feedback and state transformation. The size of this maximum feedback linearisable subsystem is greater than that of a TWIP, which has a maximum relative degree of 4 [10].

## IV. Partial Feedback Linearisation

Feedback linearisation is a procedure by which a nonlinear system can be transformed into an equivalent fully or partially linear system, achieved using a change of control input, along with either a change of state space coordinates, or a transformation of the output [13]. The extent to which a system can be linearised by these methods can be determined by examining the system's relative degree; only systems with a maximum relative degree equal to the size of their state space can be fully linearised by feedback. These methods result in a system that is either partially or fully linear, allowing the application of classical linear control and analysis techniques to a previously nonlinear plant. In the partially linearised case, the remaining nonlinear subsystems can then be controlled using nonlinear control techniques, typically an easier task than applying these techniques to the original higher dimensional nonlinear system.

Feedback linearisation of systems with a relative degree of less than $n$ will yield systems that contain zero dynamics, new states and dynamics that are unobservable from the new outputs, which may be unstable. In practise it can be dangerous for these unobservable states to be allowed to grow unboundedly, so their behaviour must be considered during control design.

These techniques have been applied to various forms of inverted pendulum, such as the single and double cart-pole inverted pendulums [14], [15], the reaction wheel inverted pendulum [16], the acrobot [17], [18], and most relevantly, the two-wheeled inverted pendulum [10], [19], [20]. These methods have never been applied to a ball-balancing system. As all of these systems are underactuated only partial feedback linearisation is achieved, with nonlinear controllers designed to control the remaining nonlinear dynamics.

In order to facilitate the derivation of a feedback linearising control, the input vector fields of (33) are first simplified using a change of input $v = P(x)u$ to define a new decoupled input $v$. It is found that

$$P(x) = \begin{bmatrix} g_{51} & g_{52} & g_{53} \\ g_{71} & g_{72} & g_{73} \\ g_{81} & g_{82} & g_{83} \end{bmatrix} \tag{51}$$

is nonsingular for $|\theta_p| \lesssim 2.4\,\mathrm{rad}$ for the parameters in Table I, and is therefore invertible under this condition, allowing the definition of the new input vector fields

$$\begin{bmatrix} \tilde{g}_1 & \tilde{g}_2 & \tilde{g}_3 \end{bmatrix} = \begin{bmatrix} & 0_{4\times 3} & \\ 1 & 0 & 0 \\ \tilde{g}_{61} & \tilde{g}_{62} & \tilde{g}_{63} \\ 0 & 1 & 0 \\ 0 & 0 & 1 \end{bmatrix} \tag{52}$$

where

$$\begin{bmatrix} \tilde{g}_{61} & \tilde{g}_{62} & \tilde{g}_{63} \end{bmatrix} = \begin{bmatrix} g_{61} & g_{62} & g_{63} \end{bmatrix} P(x)^{-1} \tag{53}$$

in which $(\tilde{g}_{61}, \tilde{g}_{62}) = 0$ for the parameters in Table I, and in which $\tilde{g}_{63}$ is a scalar valued function that is again smooth over $|\theta_p| \lesssim 2.4\,\mathrm{rad}$. The $\dot{x}_5$, $\dot{x}_7$, and $\dot{x}_8$ subsystems can then be linearised by the feedback

$$v_1 = w_1 - f_5(x), \quad v_2 = w_2 - f_7(x), \quad v_3 = w_3 - f_8(x) \tag{54}$$

in which $w = \begin{bmatrix} w_1 & w_2 & w_3 \end{bmatrix}^T$ is used as the new input, yielding the new drift and unchanged input vector fields

$$\tilde{f}(x) = \begin{bmatrix} \cos(x_3)x_5 - \sin(x_3)x_6 \\ \sin(x_3)x_5 + \cos(x_3)x_6 \\ x_7 \\ x_8 \\ 0 \\ f_6 - \tilde{g}_{61}(x_4)f_5(x) - \tilde{g}_{62}(x_4)f_7(x) \\ \qquad\qquad - \tilde{g}_{63}(x_4)f_8(x) \\ 0 \\ 0 \end{bmatrix} \tag{55}$$

$$\begin{bmatrix}\tilde{g}_1(x_4)^T\\ \tilde{g}_2(x_4)^T\\ \tilde{g}_3(x_4)^T\end{bmatrix}^T = \begin{bmatrix}0_{1\times4} & 0_{1\times4} & 0_{1\times4}\\ 1 & 0 & 0\\ \tilde{g}_{61}(x_4) & \tilde{g}_{62}(x_4) & \tilde{g}_{63}(x_4)\\ 0 & 1 & 0\\ 0 & 0 & 1\end{bmatrix} \tag{56}$$

In order for the coordinates $x$ to fully span $\mathbb{R}^8$ they must be linearly independent, meaning their gradients $\dot{x}$ must be linearly independent of one another [6]. Clearly in (55)-(56) this property has been lost, as $\dot{x}_6$ is now a linear function of $\dot{x}_5$, $\dot{x}_7$, and $\dot{x}_8$. A state transformation $\mathrm{T} : x \to z$ is therefore required to transform $x$ into some new set of linearly independent coordinates $z$ as $z = \mathrm{T}(x)$. As $\dot{x}_i$ for $i = [1\ ..\ 5, 7, 8]$ are already linearly independent, these can be mapped as $z_i = x_i$. As $w \equiv \begin{bmatrix}\dot{x}_5 & \dot{x}_7 & \dot{x}_8\end{bmatrix}^T$, it is required that

$$\frac{\partial z_6}{\partial x}\begin{bmatrix}\tilde{g}_1(x_4) & \tilde{g}_2(x_4) & \tilde{g}_3(x_4)\end{bmatrix} = 0 \tag{57}$$

Writing $\nabla z_6 = \begin{bmatrix}\alpha_1 & \dots & \alpha_8\end{bmatrix}$, by (57) it is implied that

$$\alpha_5 + \alpha_6\tilde{g}_{61} = 0,\ \ \alpha_7 + \alpha_6\tilde{g}_{62} = 0,\ \ \alpha_8 + \alpha_6\tilde{g}_{63} = 0 \tag{58}$$

which is satisfied for

$$\alpha_5 = -\lambda\tilde{g}_{61},\ \ \alpha_6 = \lambda,\ \ \alpha_7 = -\lambda\tilde{g}_{62},\ \ \alpha_8 = -\lambda\tilde{g}_{63} \tag{59}$$

Choosing $\lambda = 1$, $z_6$ can be defined as

$$z_6 = x_6 - x_5\tilde{g}_{61} - x_7\tilde{g}_{62} - x_8\tilde{g}_{63} \tag{60}$$

defining the transformation $\mathrm{T}(x)$ as

$$z = \mathrm{T}(x) = \begin{bmatrix}x_1\\ \vdots\\ x_5\\ x_6 - x_5\hat{g}_{61} - x_7\hat{g}_{62} - x_8\hat{g}_{63}\\ x_7\\ x_8\end{bmatrix} \tag{61}$$

Again for the parameters in Table I

$$\det\left(\frac{\partial \mathrm{T}(x)}{\partial x}\right) \neq 0\ \forall\ \{x \in \mathbb{R}^8 \mid x_4 \bmod 2\pi \not\approx \pm 2.4\} \tag{62}$$

therefore the Jacobian of T is locally invertible, meaning T is a local diffeomorphism under this condition [6], with an inverse mapping $x = \mathrm{T}^{-1}(z)$. Taking the differential of $\mathrm{T}(x)$ w.r.t. time allows $\dot{z}$ to be expressed in terms of $x$ as

$$\dot{z}_i = \dot{x}_i, \quad i = [1, \dots, 5, 7, 8] \tag{63}$$

$$\dot{z}_6 = -\dot{x}_5\tilde{g}_{61} - x_5\frac{\partial\tilde{g}_{62}}{\partial x_4} - \dot{x}_7\tilde{g}_{62} - x_7\frac{\partial\tilde{g}_{62}}{\partial x_4} - \dot{x}_8\tilde{g}_{63} - x_8\frac{\partial\tilde{g}_{63}}{\partial x_4} \tag{64}$$

which when substituted with differentials of $x$ from (55) yields the new set of dynamic equations

$$\dot{z}_1 = \cos(z_3)z_5 - \sin(z_3)(z_6 + z_5\tilde{g}_{61}(z) + z_7\tilde{g}_{62}(z) + z_8\tilde{g}_{63}(z)) \tag{65}$$

$$\dot{z}_2 = \sin(z_3)z_5 + \cos(z_3)(z_6 + z_5\tilde{g}_{61}(z) + z_7\tilde{g}_{62}(z) + z_8\tilde{g}_{63}(z)) \tag{66}$$

$$\dot{z}_3 = z_7 \tag{67}$$

$$\dot{z}_4 = z_8 \tag{68}$$

$$\dot{z}_5 = w_1 \tag{69}$$

$$\dot{z}_6 = f_6(z) - z_5\frac{\partial\tilde{g}_{61}(z)}{\partial z_4} - z_7\frac{\partial\tilde{g}_{62}(z)}{\partial z_4} - z_8\frac{\partial\tilde{g}_{63}(z)}{\partial z_4} - \tilde{g}_{61}(z_4)f_5(z) - \tilde{g}_{62}(z_4)f_7(z) - \tilde{g}_{63}(z_4)f_8(z) \tag{70}$$

$$\dot{z}_7 = w_2 \tag{71}$$

$$\dot{z}_8 = w_3 \tag{72}$$

where all $f(x)$ and $\tilde{g}(x)$ have been rewritten in terms of $z$ using $x = \mathrm{T}^{-1}(z)$. Under this state transformation and feedback it is evident that $w$ has been eliminated from the expression for $\dot{z}_6$, meaning $\dot{z}_6$, $\dot{z}_1$, and $\dot{z}_2$ now represent internal dynamics, and in which $\dot{z}_5$, $\dot{z}_7$, and $\dot{z}_8$ are now independent of the drift vector, and are linear and decoupled in the new input $w$.

The internal dynamics (70) are found to contain zeroth to second time derivatives of $\theta_p$, and cannot be integrated to eliminate either of these velocity or acceleration terms. This expression therefore forms a second order nonholonomic constraint, also referred to as a dynamic constraint.

Examining the zero dynamics found by setting $w = z_5 = z_7 = z_8 = 0$ in $(\dot{z}_1, \dot{z}_2, \dot{z}_6)$, and whilst assuming defined roller angles, wheel spacing symmetry, and zero friction for sake of model simplification, yields

$$\dot{z}_1 = -z_6\sin(z_3) \tag{73}$$

$$\dot{z}_2 = z_6\cos(z_3) \tag{74}$$

$$\dot{z}_6 = -\frac{gh_pm_pr_w\sin(z_4)}{4I_{wx} + m_pr_w^2 + 4m_wr_w^2 + h_pm_pr_w\cos(z_4)} \tag{75}$$

in which it is clear that the zero dynamics do not have a stable equilibrium for $z_4 \neq 0$, and so the system is non-minimum phase [21].

To summarise, through input transformation, coordinate transformation, and nonlinear feedback, the nonlinear system (28) has been transformed into an equivalent system of five linear and three nonlinear ODEs, with new input $w \equiv \begin{bmatrix}\dot{v}_x & \ddot{\phi} & \ddot{\theta}_p\end{bmatrix}^T$. Actual motor torques are retrieved by the mapping $w \to v \to u \to \tau$. The simulated response of this system to a $0.25\,\mathrm{Hz}$ square wave input of unit amplitude to each of $w$ is shown in Fig. 3, demonstrating the correct linear response of the feedback linearised subsystems $v_x$, $\dot{\phi}$, and $\dot{\theta}_p$, and unbounded growth of $v_y$ as expected.

## V. Nonlinear Control of the Partially Feedback Linearised CMD

Three separate CMD controllers are now to be derived. The first of these is to control the CMD's local frame body velocities, useful in applications where the CMD is to be 'driven'

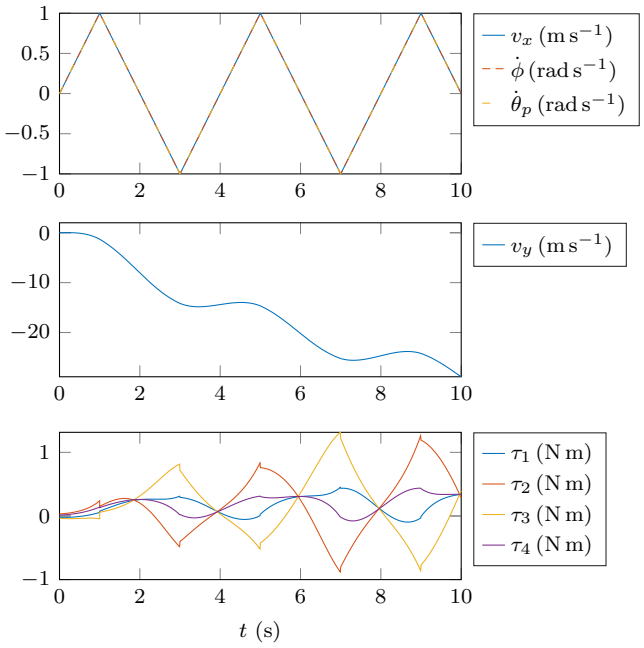


Fig. 3. Simulated state trajectories of the partially feedback linearised CMD, initialised at the origin and with each of $w$ driven by a 0.25 Hz square wave of unit amplitude. This demonstrates the expected triangular velocity profile in the $v_x$, $\dot{\phi}$, and $\dot{\theta}_p$ states, while $v_y$ grows unboundedly. The required wheel torque trajectories $\tau$ remain well defined, as the singularity in (52) is avoided.

by a user, such as when operating as a personal mobility or teleoperated platform. The second controller is to control system velocities in the fixed inertial frame, and the third and final is to control the position of the CMD in the fixed inertial frame. These are more useful in situations where the CMD is to operate autonomously, such as when navigating a map. Both velocity controllers must incorporate lean angle and body acceleration constraints to ensure the generation of smooth trajectories between distant references, and to approximately bound wheel torques. The inertial frame position controller must additionally enforce velocity constraints to bound the system's kinetic energy when performing distant translations.

Pathak controls a partially feedback linearised two-wheeled inverted pendulum using a backstepping approach [10]. In this method a cascade nonlinear system is controlled by recursively stabilising each subsystem whilst 'stepping back' through the cascaded subsystems. This stabilisation is performed by deriving controllers that yield closed-loop subsystems that can be formulated as Lyapunov functions, yielding control of the overall system with stability and convergence guarantees for the full nonlinear dynamics. Constraints can be incorporated using Lyapunov barrier functions [22], scalar functions in which a unique minimum is attained at the desired steady state, and which tend to infinity as the constraint is approached. This allows an embedding of constraints directly into the control law, whilst retaining a stability proof for the closed-loop system. These methods can therefore be used to derive the required nonlinear controllers for the CMD, whilst maintaining stability for the full set of feasible references.

### A. Backstepping Control of Local Body Frame Velocities

This controller is required to drive the system local body frame velocities $(v_x, v_y, \dot{\phi})$ to setpoints $(v_{xr}, v_{yr}, \dot{\phi}_r)$. This must be performed whilst bounding deviation of $\theta_p$ from zero so as to avoid attempting to translate using slip-inducing lean angles, and accelerations $\dot{v}_x$ and $\ddot{\phi}$ must be bounded to again avoid inducing wheel slip. Such a controller would be useful in applications where a user wishes to 'drive' the system, for example if such a system were used as a personal vehicle or teleoperated platform.

Control is to be split into two layers. The first layer is to provide aggressive control of the $\theta_p$ subsystem to provide high bandwidth resistance to disturbance, especially that generated by varying friction forces when translating in the $b_x$ direction. This is achieved using the linear controller

$$w_3 = -K_{\dot{\theta}_p}\dot{\theta}_p - K_{\theta_p}(\theta_p - \theta_{pr}) \tag{76}$$

with suitable gains $K_{\dot{\theta}_p}$ and $K_{\theta_p}$, providing global exponential convergence $\theta_p \to \theta_{pr}$, where $\theta_{pr}$ represents a new internal reference signal. As this subsystem has relatively fast dynamics, and as low-noise measurements of $\dot{\theta}_p$ and $\theta_p$ are available, high gains can be used to allow for high bandwidth reference tracking. While linear controllers could also be used to control the feedback linearised $v_x$ and $\dot{\phi}$ subsystems, these are instead to be controlled by the outer loop as to allow the embedding of acceleration constraint enforcement. Constraints on $w_3$ are to be approximately enforced in the generation of the new $\theta_{pr}$ reference signal.

The goal of the outer controller is to generate $w_1$, $w_2$, and $\theta_{pr}$ trajectories that result in convergence of $(v_x, v_y, \dot{\phi}) \to (v_{xr}, v_{yr}, \dot{\phi}_r)$ within finite time. Unlike a TWIP, cross coupling between the $(\theta_p, v_y)$ subsystem and the $v_x$ and $\dot{\phi}$ subsystems, for example acceleration forces acting on $\theta_p$ when $v_x\dot{\phi} \neq 0$, means that $\theta_{pr} \not\to 0$ may be required for $\dot{v}_y \to 0$ in steady state.

From (55), acceleration $\dot{v}_y$ can be expressed as

$$\begin{aligned}\dot{v}_y = f_{\dot{v}_y}(x, w) = f_6(x) - \hat{g}_{61}(x)f_5(x) - \hat{g}_{62}(x)f_7(x) \\ - \hat{g}_{63}(x)f_8(x) + \hat{g}_{61}(x)w_1 + \hat{g}_{62}(x)w_2 + \hat{g}_{63}(x)w_3\end{aligned} \tag{77}$$

This is a complex expression for which it is difficult to analyse the effect of parameter choice, so this is instead substituted with the parameters in Table I, with the assumption that the properties of this function are unlikely to significantly change over realistic ranges of parameter variation. This yields an expression of the form

$$\begin{aligned}f_{\dot{v}_y}(x, w) = aw_3 - v_x\dot{\phi} - b\sin(\theta_p)\dot{\phi}^2 \\ + \frac{cw_3 - dv_y + \sin(\theta_p)\left(e\dot{\phi}^2 - f\dot{\theta}_p^2 - g\right) + hv_x\dot{\phi}}{\cos(\theta_p) + i}\end{aligned} \tag{78}$$

where $0 < e \ll \{a, b, f, h\} \ll \{c, d, i\} \ll g$, in which the operator $\ll$ denotes a difference of approximately an order of magnitude. For the prototype's parameters given in Table I these coefficients evaluate to $a = 0.03$, $b = 0.072$, $c = 0.20$, $d = 0.13$, $e = 0.0091$, $f = 0.030$, $g = 9.8$, $h = 0.038$, and $i = 0.54$. For comparison the same analysis of coefficients is performed for a taller and heavier system with $h_p = 1$, $m_p =$

20, $I_{px} = 20$, yielding coefficients of approximate magnitude $0 < h \ll \{d, e\} \ll \{a, f, i\} \ll \{b, c\} \ll g$. Importantly, while some coefficients change in magnitude relative to one another, the constant $g$ remains significantly larger than all other coefficients.

Equation (78) has no analytical solution for $\theta_p$. However, arranging it into the form $0 = f(x, w, \dot{v}_y)$ and examining $f(x, w, \dot{v}_y)$ for $\theta_p = \pm\pi/2$ yields

$$f(x, w, \dot{v}_y) = \frac{a}{i} w_3 - \frac{d}{i} v_y - \dot{v}_y - \left(1 - \frac{h}{i}\right) \dot{\phi} v_x \mp \left(b - \frac{e}{i}\right) \dot{\phi}^2 \mp \frac{f}{i} \dot{\theta}_p^2 \mp \frac{g}{i}, \quad \text{for } \theta_p = \pm\pi/2 \tag{79}$$

Equation (78) is a continuous smooth function over the interval $\theta_p \in (-\cos^{-1}(-i), \cos^{-1}(-i))$. By the intermediate value theorem as long as for a given $\{x, w_3, \dot{v}_y\} \in \mathbb{R}^7 \times \mathbb{R} \times \mathbb{R}$ (79) is of opposite sign for $\theta_p = \pi/2$ and $\theta_p = -\pi/2$, there must exist some intermediate value of $\theta_p$ for which $f(x, w, \dot{v}_y) = 0$, i.e. a solution to (78) must exist. This condition is necessary for there to exist an inverse function $\theta_p = f^{-1}_{\dot{v}_y}(x, w_3, \dot{v}_y)$ that can be used to determine the lean angle required to achieve a given $\dot{v}_y$ for some state $x$ and input $w$, though the existence of this inverse also requires a unique mapping. The condition under which at least one solution exists for $|\theta_p| \leq \pi/2$ can be written as

$$\left| a w_3 - d v_y - i \dot{v}_y - (i - h) \dot{\phi} v_x \right| \leq (bi - e) \dot{\phi}^2 + f \dot{\theta}_p^2 + g \tag{80}$$

It is apparent that the large constant term $g$ on the rhs means this inequality is satisfied for a large set of accelerations $\dot{v}_y$ and $w_3$, of which the origin is strictly within the interior, provided the $\dot{\phi} v_x$ and $v_y$ terms are not driven excessively large. Satisfaction of this condition can therefore be guaranteed by suitably bounding the user reference inputs $\dot{v}_{xr}$ and $\dot{\phi}_r$, whilst through controller design ensuring a suitable bounding of $w_3$ and $\dot{v}_y$. While a larger feasible set could be achieved by allowing $\theta_p \in [-\cos^{-1}(i), \cos^{-1}(i)]$, as this requires intersection with the pendulum CoM and the ground this bound on $\theta_p$ is sensible, and simplifies analysis.

It is also found that $\frac{\partial \dot{v}_y}{\partial \theta_p} < 0 \ \forall \ \theta_p \in [-\frac{\pi}{2}, \frac{\pi}{2}]$ for a similar set of states and inputs, meaning (55) is monotonic in $\theta_p$, and therefore the solution to $f^{-1}_{\dot{v}_y}(x, w, \dot{v}_y)$ is guaranteed to be unique. The inverse function $f^{-1}_{\dot{v}_y}(x, w, \dot{v}_y)$ is therefore guaranteed to exist for $\theta_p \in [-\pi/2, \pi/2]$ under condition (79). $f^{-1}_{\dot{v}_{y,ss}}(x, w, \dot{v}_y)$ can be solved using the Newton-Raphson method with an analytically derived Jacobian, yielding solutions in the region of microseconds.

Steady state acceleration $\dot{v}_{y,ss}$ for a given steady state value of $\theta_p$ can be found by substituting (77) with $w_3 = \dot{\theta}_p = 0$, yielding the function $f_{\dot{v}_{y,ss}}(x, w)$, with inverse $f^{-1}_{\dot{v}_{y,ss}}(x, w, \dot{v}_{y,ss})$ later written as $f^{-1}_{\dot{v}_{y,ss}}(\dot{v}_y)$ for brevity.

**Remark 2.** *Absence of oddness property of $f_{\dot{v}_{y,ss}}(x, w)$ in $\theta_p$*

*In Pathak's [10] backstepping control of a TWIP it is shown that the TWIP's expression for steady state acceleration $f_{\dot{v}_{y,ss}}(x, w)$ is odd in $\theta_p$, such that $\theta_p f_{\dot{v}_{y,ss}}(x, w) \geq 0 \ \forall \ \theta_p \in [-\pi, \pi]$. This property requires the assumption that $\dot{\phi} = 0$.*

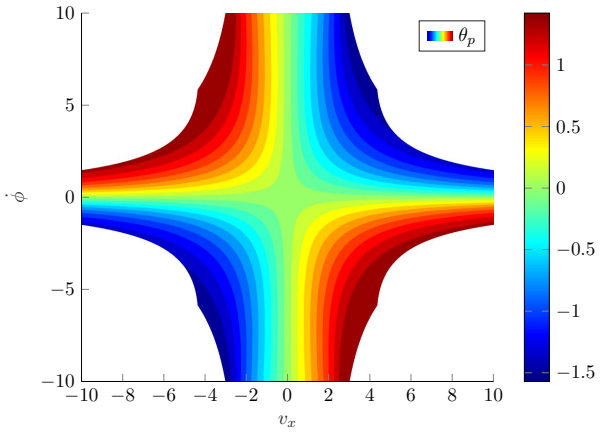


Fig. 4. A cross-section of $\mathcal{A}_{ss}$ through $v_x$ and $\dot{\phi}$ for $\dot{v}_{y,ss} = 0$, $v_y = 0$, with colour encoding the $\theta_{p,ss}$ dimension of $\mathcal{A}_{ss}$. The accessible acceleration space under a lean angle constraint $|\theta_p| \leq \bar{\theta}_p$ can be examined by considering a subset of this space.

*In order for any stability proof that relies on this oddness property to remain valid, such as that demonstrated by this author, it is therefore necessary for the system to perform control of the $\phi$ and $v_y$ subsystems separately such that $\dot{\phi}\dot{\theta}_p = 0$. The CMD is required to perform these movements simultaneously, invalidating this assumption. Also, the function $f_{\dot{v}_{y,ss}}(x, w)$ for this system contains two significant even terms $v_x\dot{\phi}$. This oddness property therefore does not extend to the CMD and so cannot be exploited for Lyapunov function derivation, necessitating a different approach to that used by Pathak [10].*

**Remark 3.** *Velocity equilibria in the local body frame.*

*For this controller it is desired for the system's local frame body velocities to converge to some user controlled reference velocities $v_{xr}$, $v_{yr}$, and $\dot{\phi}_r$, with no interest in position states other than $\theta_p$. Defining the reduced state vector $\tilde{x} = \begin{bmatrix}\theta_p & v_x & v_y & \dot{\phi} & \dot{\theta}_p\end{bmatrix}^T$ and examining $\dot{\tilde{x}} = 0$ in (55) shows these equilibria exist at any $w = 0$, $\dot{\theta}_p = 0$, $\{\theta_p, v_x, v_y, \dot{\phi}\} \in \mathcal{A}_{ss}$, where $\mathcal{A}_{ss}$ is defined as the set of $\{v_x, v_y, \dot{\phi}\}$ for which solutions to $f_{\dot{v}_{y,ss}}(x) = 0$ exist. A cross-section of this set is shown in Fig. 4, taken through $v_x$ and $\dot{\phi}$ for $v_y = 0$, with parameters from Table I. Note while $f_{\dot{v}_{y,ss}}$ also contains a $v_y$ term, it vanishes when friction is negated and has a very small coefficient, and so does not represent significant dynamics. This figure is therefore largely invariant in $v_y$, and in reality a sufficiently large $v_y\dot{\phi}$ term would result in rotation of the system about $\hat{b}_y$ and a subsequent loss of traction long before the shape of this cross-section is significantly altered.*

*To summarise, a steady state equilibrium can be obtained for any $\{\theta_p, v_x, v_y, \dot{\phi}\} \in \mathcal{A}_{ss}$, where $\mathcal{A}_{ss}$ is a large set centered about the origin. It is therefore feasible for this controller to achieve the asymptotic tracking $\{v_x, v_y, \dot{\phi}\} \to \{v_{xr}, v_{yr}, \dot{\phi}_r\}$ as $t \to \infty$.*

With the $\theta_p$ subsystem globally asymptotically stabilised by linear feedback, the outer loop is required to generate suitable $\theta_{pr}$, $w_1$, and $w_2$ trajectories that yield the asymptotic

tracking $(v_x, v_y, \dot{\phi}) \rightarrow (v_{xr}, v_{yr}, \dot{\phi}_r)$. These subsystems have substantially slower dynamics than the $\theta_p$ subsystem, allowing the assumption that the linear inner loop has converged, i.e. $\theta_p = \theta_{pr}$ and $\dot{\theta}_p = w_3 = 0$. While the $v_x$ and $\dot{\phi}$ subsystems have been rendered linear by feedback linearisation, a non-linear controller is still used in order to allow the embedded enforcement of the constraints $|w_1| \leq \overline{w}_1$ and $|w_2| \leq \overline{w}_2$. These constraints act to make the resulting control laws favour smooth steady accelerations over aggressive acceleration impulses during a step reference change, and can therefore be used to alleviate the risk of wheel slip by acting as an analogue for a wheel torque constraint.

Consider the Lyapunov function candidate

$$V_\Sigma = \frac{\left(\theta_{pr} - f^{-1}_{\dot{v}_{y,ss}}(0)\right)^2}{2\left(\overline{\theta}_p^2 - \theta_{pr}^2\right)} + \frac{K_v\left((v_{xr} - v_x)^2 + (v_{yr} - v_y)^2\right)}{2} + \frac{K_{\dot{\phi}}(\dot{\phi}_r - \dot{\phi})^2}{2} + \frac{1}{2\left(\overline{w}_1^2 - w_1^2\right)} + \frac{1}{2\left(\overline{\dot{\phi}}^2 - w_2^2\right)} \quad (81)$$

The first term of (81) has a unique minimum at $f^{-1}_{\dot{v}_{y,ss}}(0) = \theta_{pr}$, i.e. it is minimised when $\theta_{pr}$ has converged to the steady-state lean angle $\theta_{p,ss}$ required to maintain $\dot{v}_y = 0$, found by solution of $\theta_{p,ss} = f^{-1}_{\dot{v}_{y,ss}}(0)$, whilst tending to infinity as $\theta_{pr} \rightarrow \pm\overline{\theta}_{pr}$, bounding $\theta_{pr}$. The second and third terms have unique minimums at $v_y = v_{yr}$, $v_x = v_{xr}$, and $\dot{\phi} = \dot{\phi}_r$, with a quadratic cost on deviation from these minima. The final two terms act as barrier functions to enforce $|w_1| \leq \overline{w}_1$ and $|w_2| \leq \overline{w}_2$, with minimums at $w_1 = 0$ and $w_2 = 0$. $V_\Sigma$ is therefore globally positive semidefinite when constraints are satisfied and $\left(K_v, K_{\dot{\phi}}\right) > 0$, i.e. $V_\Sigma \geq 0$, has a single unique minimum, and by inspection is radially unbounded for states within the constrained set, but is bounded for $\theta_{pr} \rightarrow \infty$ as the first term of (81) converges to 1. As these conditions are not met for states outside of the constraints, care must be taken to initialise the system with constraints satisfied, i.e. the controller is not able to recover from a constraint violation. However, as the constrained signals exist purely internally this will never occur.

Consider the control laws

$$\dot{\theta}_{pr} = \frac{-\dot{f}^{-1}_{\dot{v}_{y,ss}}(0)\left(\overline{\theta}_p^2 - \theta_{pr}^2\right)}{\left(f^{-1}_{\dot{v}_{y,ss}}(0)\theta_{pr} - \overline{\theta}_p^2\right)} - K_r\left(\theta_{pr} - f^{-1}_{\dot{v}_{y,ss}}(0)\right)\left(f^{-1}_{\dot{v}_{y,ss}}(0)\theta_{pr} - \overline{\theta}_p^2\right) + \frac{\left(\overline{\theta}_p^2 - \theta_{pr}^2\right)^2 K_v f_{\dot{v}_{y,ss}}(\theta_{pr})(v_{yr} - v_y)}{\left(\theta_{pr} - f^{-1}_{\dot{v}_{y,ss}}(0)\right)\left(f^{-1}_{\dot{v}_{y,ss}}(0)\theta_{pr} - \overline{\theta}_p^2\right)} \quad (82)$$

$$\dot{w}_1 = -K_{w_1} w_1 + K_v(v_{xr} - v_x)\left(\overline{w}_1^2 - w_1^2\right)^2 \quad (83)$$

$$\dot{w}_2 = -K_{w_2} w_2 + K_{\dot{\phi}}(\dot{\phi}_r - \dot{\phi})\left(\overline{w}_2^2 - w_2^2\right)^2 \quad (84)$$

By substituting (82)-(84) into $\dot{V}_\Sigma$ it is found that $\dot{V}_\Sigma \leq 0$ for $(K_r, K_{w_1}, K_{w_2}) > 0$, thus proving closed-loop stability. This stability proof does, however, require $\{v_{xr}, v_{yr}, \dot{\phi}_r\} \in \mathcal{A}_{ss}$, $x_0 \in \mathcal{A}_{ss}$, and $x \in \left\{\mathcal{A}_{ss} \ : |\theta_p| \leq \overline{\theta}_p\right\} \ \forall \ t$. While the first two conditions can be trivially ensured, the latter cannot be guaranteed, as any overshoot when approaching references that require $\theta_{p,ss}$ to lie close to $\overline{\theta}_p$ could violate this condition. This can be addressed by bounding the solution to $f^{-1}_{\dot{v}_{y,ss}}(0)$.

Using LaSalle's invariance principle it is apparent that

$$\lim_{t\rightarrow\infty} \begin{cases} \theta_{p,r} = f^{-1}_{\dot{v}_{y,ss}}(0) \implies v_y = v_{yr} \\ w_1 = 0 \implies v_x = v_{xr} \\ w_2 = 0 \implies \dot{\phi} = \dot{\phi}_r \end{cases} \quad (85)$$

thus guaranteeing asymptotic convergence to the desired references.

The dynamics of the controller can be tuned by modification of the 'damping' terms $K_r$, $K_{w_1}$, and $K_{w_2}$, and 'proportional' terms $K_v$ and $K_{\dot{\phi}}$. Convergence of the expression

$$\lim_{\theta_{pr}\rightarrow f^{-1}_{\dot{v}_{y,ss}}(0)} \frac{f_{\dot{v}_{y,ss}}(\theta_{pr})}{\left(f^{-1}_{\dot{v}_{y,ss}}(0) - \theta_{pr}\right)} \quad (86)$$

in the latter term of (82) cannot be directly determined, as performing the substitution $\theta_{pr} = f^{-1}_{\dot{v}_{y,ss}}(0)$ yields an indeterminate expression. However, as these functions are known to be continuously differentiable within the operating region of interest, convergence can instead be proven by L'Hôpital's rule, and thus the control law (82) remains defined.

Finally, all that remains to be proven is that (86) does not converge to zero within the operating region of interest, as if this were the case the third term of (82) would vanish at $\theta_{pr} = f^{-1}_{\dot{v}_{y,ss}}(0)$, even if $v_y \neq v_{yr}$. As the first term of this control law vanishes when $w_1 = w_2 = 0$, and the second term also vanishes when $\theta_{pr} = f^{-1}_{\dot{v}_{y,ss}}(0)$, this would force $\dot{\theta}_{pr} = 0 \ \forall \ t \rightarrow \infty$, and thus prevent any further control action even when $v_y \neq v_{yr}$. This can be proven numerically using the Monte Carlo method, finding this expression to be negative definite for $|\theta_p| \lessapprox 1.2\,\mathrm{rad}$. This is a tighter bound on $\theta_p$ than found previously, but still far larger than is expected to be attained in practice.

As this stability proof relies on the assumption of prior convergence of the inner $\theta_p \rightarrow \theta_{pr}$ control loop, update of the control law (82) should be avoided when $|\theta_p - \theta_{pr}| \gg 0$. This can be achieved by multiplication of (82) by the expression

$$e^{-K|\theta_p - \theta_{pr}|} \quad (87)$$

where $K \gg 1$. This prevents substantial change of $\theta_{pr}$ when the inner loop is still converging.

Fig. 5 shows the simulated response of the prototype system with this controller to a reference $(v_{xr}, v_{yr}, \dot{\phi}_r) = (1, 1, 4)$, initialised at the origin. This shows asymptotic convergence to the reference whilst satisfying $\theta_p$, $w_1$, and $w_2$ constraints, with $\theta_p$ correctly converging to the required steady state $\theta_p = \theta_{p,ss} = f^{-1}_{\dot{v}_{y,ss}}(0)$. The error $\theta_p - \theta_{pr}$ remains small, indicating that (87) functions as intended and thus the assumption of convergence of this inner loop holds, with full convergence achieved in steady state.

Fig. 6 shows the experimental response of the prototype to a reference $(v_{xr}, v_{yr}, \dot{\phi}_r) = (0, 1, 2)$, again initialised at the origin. A more conservative reference is chosen than that used

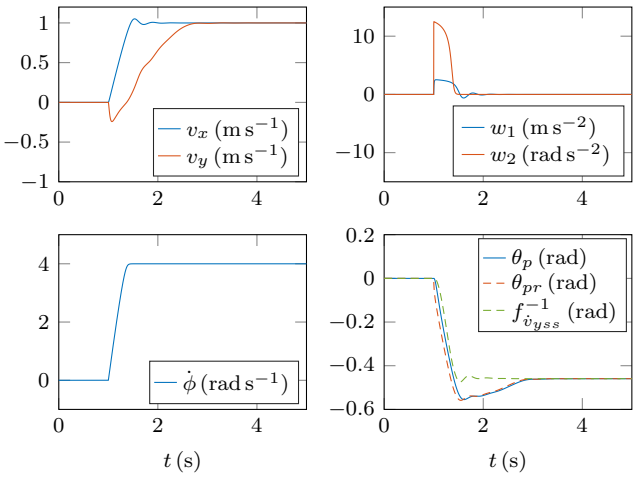


Fig. 5. Simulated system state trajectories over time for a reference $(v_{xr}, v_{yr}, \dot{\phi}_r) = (1, 1, 4)$, initialised at the origin with $\overline{\theta}_p = 0.6$, $\overline{w}_1 = 2$, and $\overline{w}_2 = 4$. This shows asymptotic convergence to the reference whilst satisfying $\theta_p$, $w_1$, and $w_2$ constraints, with $\theta_p$ correctly converging to the required steady state $\theta_p = \theta_{p,ss} = f^{-1}_{\dot{v}_{yss}}(0)$. The error $\theta_p - \theta_{pr}$ remains small, indicating that (87) functions as intended and thus the assumption of convergence of this inner loop holds, with full convergence achieved in steady state.

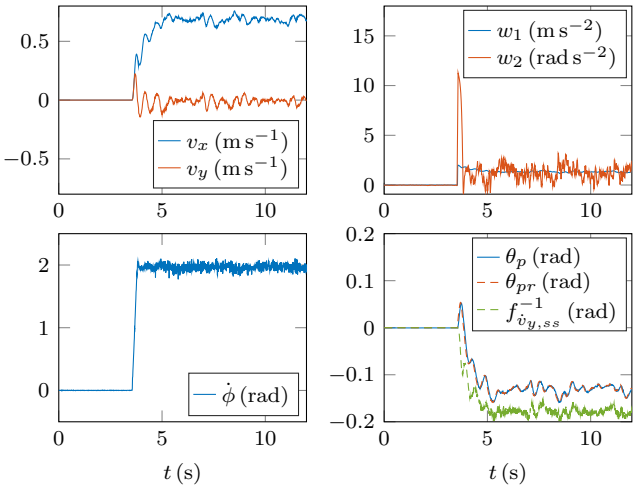


Fig. 6. Experimental system state trajectories for a reference $(v_{xr}, v_{yr}, \dot{\phi}_r) = (1, 0, 2)$, initialised at the origin with $\overline{\theta}_p = 0.4$, $\overline{w}_1 = 3$, and $\overline{w}_2 = 15$. This shows good tracking of $\theta_p \to \theta_{pr}$, however, now $\theta_{pr} \not\to f^{-1}_{\dot{v}_{y,ss}}(0)$. This is found to be due to imperfect tracking within the inner loop yielding a steady state bias in $w_3$, which is in turn due to imperfect feedback linearisation. A combination of this and further model error yields a steady state tracking error of the $v_{xr}$ and $v_{yr}$ references, though in reality this is visually imperceptible.

in simulation, as wheel slip is found to occur before the more aggressive reference can be reached. This results in the system following a circular trajectory whilst maintaining a constant nonzero lean angle.

A small steady state tracking error, though hard to discern in this figure, is present in the linear $\theta_p \to \theta_{pr}$ controller. This is to be expected, as no model can perfectly describe the behaviour of a real-world system due to parameter uncertainty and unmodelled dynamics, meaning a model-derived feedback linearisation will always be imperfect and therefore not converge. This manifests as a steady state tracking error $\theta_p \to \theta_{pr} + e$, and due to the proportional feedback term in this controller results in a non-zero steady state $w_3$, i.e. $w_3 \to K_{\theta_p} e \neq 0$. This invalidates the assumption in the definition of $f^{-1}_{\dot{v}_{y,ss}}(\dot{v}_y)$, yielding the steady state bias in the solution to $f^{-1}_{\dot{v}_{y,ss}}$, visible in this figure. A significant steady-state tracking error is visible in the $v_x \to v_{xr}$ controller, and $w_1 \not\to 0$. This again indicates an error in the feedback linearisation, as while $w_1 \neq 0$ the velocity $v_x$ reaches a steady state. This could be addressed by improved friction modelling in the underlying model, as to predict this force resisting $w_1$ in steady state, or by some form of integral action.

### B. Backstepping Inertial Frame Velocity Control

Control of inertial frame velocities $\dot{x}$ and $\dot{y}$ is more useful in applications that involve the autonomous navigation of an environment. The desired steady state body accelerations are now defined as $\dot{v}_x = \dot{\phi} v_y$ and $\dot{v}_y = -\dot{\phi} v_x$, representing unforced body acceleration due to the mapping of inertial frame velocities into the rotating local frame.

**Remark 4.** *Inertial frame velocity equilibria*

*For an inertial frame velocity controller it is desired that the inertial frame body velocities $\{\dot{x}, \dot{y}, \dot{\phi}\}$ asymptotically converge to the references $\{\dot{x}_r, \dot{y}_r, \dot{\phi}_r\}$ within finite time. In steady state the local frame body accelerations must therefore be purely that due to rotation of inertial frame velocities into the local body frame, i.e. $\dot{v}_x = \dot{\phi} v_y$, $\dot{v}_y = -\dot{\phi} v_x$, and local frame body velocities must be simply a rotation of the time invariant inertial frame velocity reference into the local frame, so*

$$\begin{bmatrix} v_x \\ v_y \end{bmatrix} = R^T_{EB} \begin{bmatrix} \dot{x} \\ \dot{y} \end{bmatrix} = \begin{bmatrix} \cos(\phi)\dot{x} + \sin(\phi)\dot{y} \\ -\sin(\phi)\dot{x} + \cos(\phi)\dot{y} \end{bmatrix} \tag{88}$$

*In steady state it is therefore required that $\dot{x} = \dot{x}_r$ and $\dot{y} = \dot{y}_r$, which for time invariant references implies $(\ddot{x}, \ddot{y}) \to 0$. It is also required that $\dot{\phi} = \dot{\phi}_r$, so $\phi = \dot{\phi}_r t$ in steady state, and it is assumed that $\phi_0 = 0$.*

*Expressing inertial frame body accelerations in terms of inertial frame velocities, the local body frame acceleration term $\dot{v}_y$, and performing the above substitutions, yields*

$$\begin{bmatrix} \ddot{x} \\ \ddot{y} \end{bmatrix} = \begin{bmatrix} -\sin(\dot{\phi}_r t)(\dot{v}_y + \dot{\phi}_r \dot{x}_r \cos(\dot{\phi}_r t) + \dot{\phi}_r \dot{y}_r \sin(\dot{\phi}_r t)) \\ \cos(\dot{\phi}_r t)(\dot{v}_y + \dot{\phi}_r \dot{x}_r \cos(\dot{\phi}_r t) + \dot{\phi}_r \dot{y}_r \sin(\dot{\phi}_r t)) \end{bmatrix} \tag{89}$$

*Substituting $\dot{v}_y$ in* (89) *with* (78)*, solving again for $\begin{bmatrix} \ddot{x} & \ddot{y} \end{bmatrix}^T$, and equating to zero as required in steady state yields*

$$\begin{bmatrix} \ddot{x} \\ \ddot{y} \end{bmatrix} = \begin{bmatrix} \frac{-\sin(\dot{\phi}_r t)\Gamma(t)}{i + \cos(\theta_p)} \\ \frac{\cos(\dot{\phi}_r t)\Gamma(t)}{i + \cos(\theta_p)} \end{bmatrix} = \begin{bmatrix} 0 \\ 0 \end{bmatrix} \tag{90}$$

*where*

$$\begin{aligned} \Gamma(t) = {} & w_3 \left(c + ai + a\cos(\theta_p)\right) + \dot{\phi}_r \dot{y}_r h \sin(\dot{\phi}_r t) \\ & - \sin(\theta_p)\Big(g - f\dot{\theta}_p^2 + \dot{\phi}_r^2 \left(e - bi - b\cos(\theta_p)\right)\Big) \\ & + \dot{x}_r d \sin(\dot{\phi}_r t) - \dot{y}_r d \cos(\dot{\phi}_r t) + \dot{\phi}_r \dot{x}_r h \cos(\dot{\phi}_r t) \end{aligned} \tag{91}$$

*For $\dot{\phi}_r \neq 0$ these equalities clearly require $\Gamma(t) = 0$, which allows a unique solution for the required $w_3$ dynamics as*

$$w_3 = \frac{\sin(\theta_p)\Big(g + f\dot{\theta}_p^2 + \dot{\phi}_r^2\left(bi - e + b\cos(\theta_p)\right)\Big)}{c + a\cos(\theta_p) + ai} + \frac{\cos(\dot{\phi}_r t)\left(-\dot{\phi}_r\dot{x}_r h + \dot{y}_r d\right) + \sin(\dot{\phi}_r t)\left(-\dot{\phi}_r\dot{y}_r h - \dot{x}_r d\right)}{c + a\cos(\theta_p) + ai} \tag{92}$$

*For the parameters in Table I $(bi - e) \gg 0$, so*

$$\frac{\sin(\theta_p)\Big(g + \dot{\phi}_r^2 b\cos(\theta_p) + f\dot{\theta}_p^2 + \dot{\phi}_r^2(bi - e)\Big)}{c + a\cos(\theta_p) + ai} \tag{93}$$

*is an odd function within a neighbourhood of the origin for up to much larger values of $\dot{\phi}_r$ than are expected to be encountered. Any deviation of $\theta_p$ from 0 will result in a similarly signed $w_3$, making $\theta_p = 0$ an unstable equilibrium for this part of* (92)*. The $\cos(\dot{\phi}_r t)\left(-\dot{\phi}_r\dot{x}_r h + \dot{y}_r d\right) + \sin(\dot{\phi}_r t)\left(-\dot{x}_r d - \dot{\phi}_r\dot{y}_r h\right)$ expression is time varying when $\dot{\phi}_r \neq 0$, which acts to perturb* (93)*. The dynamics can therefore only be stabilised if this is achieved by this term, which given that this expression is invariant in $\theta_p$ cannot be the case. An unstable equilibrium can be achieved for the $\dot{\phi}_r = 0$ case, as this makes the latter expression time invariant, allowing a time invariant solution for $w_3$. The overall dynamics are therefore unstable for $\theta_p \in [-\frac{\pi}{2}, \frac{\pi}{2}]$, meaning that for $\ddot{x} = \ddot{y} = 0$ to be maintained when $\dot{\phi}_r \neq 0$ the system is is forced to violate the constraint $|\theta_p| < \frac{\pi}{2}$, making the asymptotic tracking of constant $\dot{x}_r$ and $\dot{y}_r$ trajectories with a time varying heading impossible.*

As from Remark 4 no states satisfying $\|v\|\dot{\phi} \neq 0$ represent equilibria, asymptotic tracking of constant inertial frame velocity references is not possible, and thus a degree of tracking error is to be expected. Like in Section V-A it is desired that $\theta_p \to f_{\dot{v}_{y,ss}}^{-1}(-v_x\dot{\phi})$, so a similar energy function to that in (81) can be used, though now this will never be perfectly tracked in steady state. Quadratic energy functions are defined with unique minimums at $\dot{x} = \dot{x}_r$ and $\dot{y} = \dot{y}_r$. However, as these minimums no longer represent equilibria of the system it is expected that the controlled system will follow a periodic trajectory about these references in steady state, with the characteristics of this limit cycle tunable by manipulation of control gains. Identical energy functions to that in (81) are used to describe a quadratic cost on $|\dot{\phi} - \dot{\phi}_r|$ and a barrier function on $w_2$. A similar barrier function is used to constrain $w_1$. As the purpose of this barrier is to constrain wheel torque demands, it makes more sense in this application to only apply the barrier to forced body acceleration, rather than also constraining acceleration due to rotation of inertial frame velocities into the local body frame. The barrier function is therefore chosen to instead enforce

$$|w_1 - v_y\dot{\phi}| < \overline{v}_{xf} \tag{94}$$

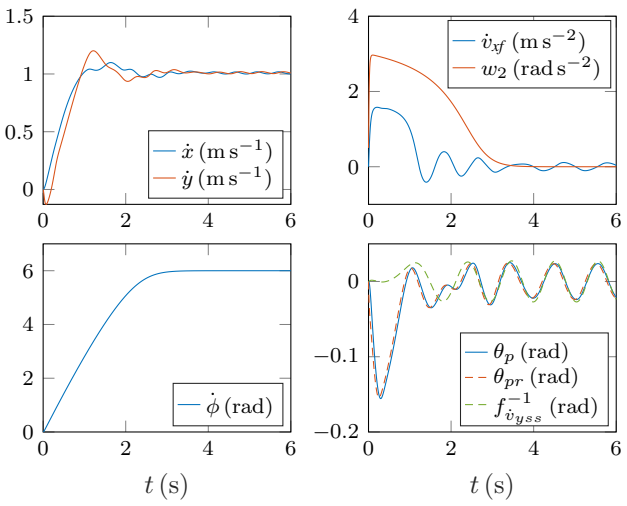


Fig. 7. Simulated system state trajectories for a reference $(\dot{x}_r, \dot{y}_r, \dot{\phi}_r) = (1, 1, 6)$, with the system initialised at the origin and with $\overline{\theta}_p = 0.4$, $\overline{v}_{xf} = 2$, and $\overline{w}_2 = 4$. $w_1 - v_x\dot{\phi}$ is shown rather than $w_1$, as this represents acceleration in the $v_x$ subsystem not due to rotation, and is the value that is constrained. $\theta_p$ is seen to converge towards $f_{\dot{v}_{yss}}^{-1}(0)$, though a small tracking error is now observed. This is due to the infeasibility of asymptotically tracking inertial velocity references, as well as the now invalid assumption of $\theta_p$ converging to a constant value, i.e. now $\dot{\theta}_p \neq 0$, $w_3 \neq 0$ in steady state. $\dot{x}$ and $\dot{y}$ are seen to converge to a small limit cycle about the target reference.

These new constraints and quadratic reference tracking costs can be captured by the Lyapunov function candidate

$$V_\Sigma = \frac{\left(\theta_{pr} - f_{\dot{v}_{y,ss}}^{-1}(-v_x\dot{\phi})\right)^2}{2\left(\overline{\theta}_p^2 - \theta_{pr}^2\right)} + \frac{(w_1 - \dot{\phi}v_y)^2}{2\left(\overline{v}_{xf}^2 - (w_1 - \dot{\phi}v_y)^2\right)} + \frac{K_v\left((\dot{x}_r - \dot{x})^2 + (\dot{y}_r - \dot{y})^2\right)}{2} + \frac{K_{\dot{\phi}}(\dot{\phi}_r - \dot{\phi})^2}{2} + \frac{1}{2\left(\overline{w}_2^2 - w_2^2\right)} \tag{95}$$

Substituting the control laws

$$\dot{\theta}_{pr} = \frac{-\dot{f}_{\dot{v}_{y,ss}}^{-1}(-v_x\dot{\phi})\left(\overline{\theta}_p^2 - \theta_{pr}^2\right)}{\left(f_{\dot{v}_{y,ss}}^{-1}(-v_x\dot{\phi})\theta_{pr} - \overline{\theta}_p^2\right)} - K_r\left(\theta_{pr} - f_{\dot{v}_{y,ss}}^{-1}(-v_x\dot{\phi})\right)\left(f_{\dot{v}_{y,ss}}^{-1}(-v_x\dot{\phi})\theta_{pr} - \overline{\theta}_p^2\right) + \frac{\left(\overline{\theta}_p^2 - \theta_{pr}^2\right)^2 K_v(f_{\dot{v}_{yss}}(\theta_{pr}) + v_x\dot{\phi})(v_{yr} - v_y)}{\left(\theta_{pr} - f_{\dot{v}_{y,ss}}^{-1}(-v_x\dot{\phi})\right)\left(f_{\dot{v}_{y,ss}}^{-1}(-v_x\dot{\phi})\theta_{pr} - \overline{\theta}_p^2\right)} \tag{96}$$

$$\dot{w}_1 = \dot{\phi}f_{\dot{v}_{yss}}(\theta_{pr}) + v_y w_2 - K_{w_1}(w_1 - \dot{\phi}v_y) + K_v \cdot \frac{(v_{xr} - v_x)\left(\overline{\dot{v}}_{xf} - \dot{\phi}v_y + w_1\right)^2\left(\overline{\dot{v}}_{xf} + \dot{\phi}v_y - w_1\right)^2}{\overline{\dot{v}}_{xf}^2} \tag{97}$$

$$\dot{w}_2 = -K_{w_2}w_2 + K_{\dot{\phi}}(\dot{\phi}_r - \dot{\phi})\left(\overline{w}_2^2 - w_2^2\right)^2 \tag{98}$$

into $\dot{V}_\Sigma$ it is found that $\dot{V}_\Sigma \leq 0\ \forall\ \{K_r, K_{w_1}, K_{w_2}\} > 0$, thus proving stability under the assumption that non-zero inertial

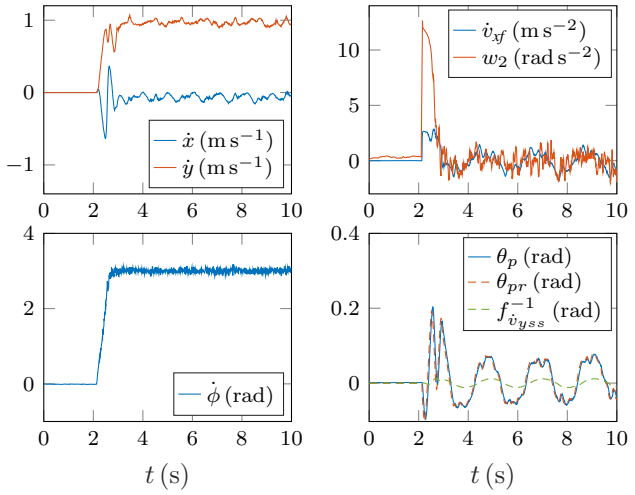


Fig. 8. Experimental system state trajectories for a reference $(\dot{x}_r, \dot{y}_r, \dot{\phi}_r) = (0, 1, 3)$, with the system initialised at the origin and with $\overline{\theta}_p = 0.4$, $\overline{\dot{v}}_{xf} = 2$, and $\overline{w}_2 = 15$. $w_1 - v_x\dot{\phi}$ is shown rather than $w_1$, as this represents acceleration in the $v_x$ subsystem not due to rotation, and is the value that is constrained. RMS $\dot{x}$ and $\dot{y}$ tracking errors of 4.2% and 7.1% are visible, due to a combination of the infeasibility of perfect tracking, imperfect feedback linearisation, and modelling error in the outer control laws.

frame velocities are attainable in steady state while $\dot{\phi} \neq 0$. As from Remark 4 this is not possible, this stability proof is invalidated, though as the necessary resulting limit cycle is expected to be small it is assumed that this stability proof is still relevant to some degree. Control gains are tuned as to achieve a desirable trade-off between control performance and minimisation of this periodic error trajectory.

As in the body velocity controller this controller also relies on the assumption $\theta_p = \theta_{pr}$, so update of the control is again slowed by multiplying the second and third terms of (96) by (87) such that the control law is slowed when the inner loop has not converged, but without affecting the first term of (96) that is required to feedforward a necessary variation in $\theta_p$ due to rotation of inertial frame velocities into the local body frame.

Fig. 7 shows the simulated response of the controlled system to a reference $(\dot{x}_r, \dot{y}_r, \dot{\phi}_r) = (1, 1, 6)$ with constraints $\overline{\theta}_p = 0.4$, $\overline{\dot{v}}_{xf} = 2$, and $\overline{w}_2 = 4$, with the system initialised at the origin. This demonstrates convergence to an acceptable velocity trajectory limit cycle with an RMS error of 4.1%, and satisfaction of the constraints $|\theta_{pr}| < \overline{\theta}_{pr}$, $|w_1 - v_x\dot{\phi}| < \overline{\dot{v}}_{xf}$, and $|w_2| < \overline{w}_2$. In steady state $\theta_p$ is seen to closely track $f^{-1}_{\dot{v}_{y,ss}}(-v_x\dot{\phi})$. Controller parameters are selected to best demonstrate the controller; more aggressive gains can obtain faster tracking without significantly altering the limit cycle.

Fig. 8 shows the experimental response of the prototype to a reference $(\dot{x}_r, \dot{y}_r, \dot{\phi}_r) = (0, 1, 3)$. This highlights a weakness in this controller; just as selection of controller gains affects the system's resulting limit cycle, this is also influenced by imperfect feedback linearisation and modelling error in the control laws, yielding larger periodic velocity tracking errors, with RMS errors of 10.8% and 7.8% respectively. From observation it is believed that the main influencing unmodelled dynamic is related to friction in the Mecanum wheel rollers,

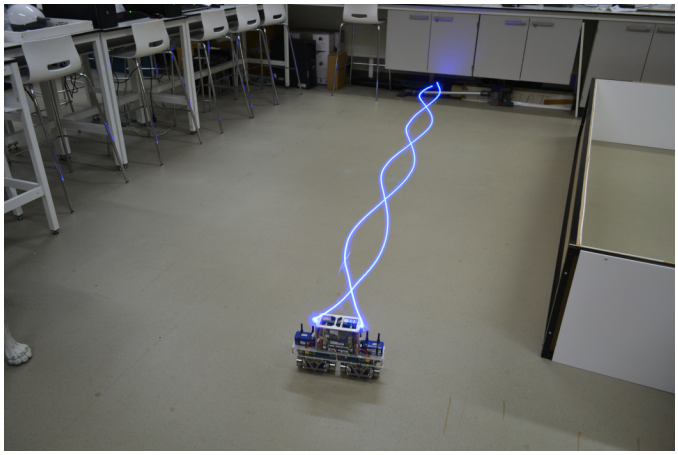

Fig. 9. A long exposure image of the trajectory in Fig. 8, in which two blue LEDs are used to capture the tracked path.

which in practise will not be perfectly modelled by the linear friction models used in this article. Fig. 9 uses a long exposure image to demonstrate this experiment.

### C. Backstepping Global Position Control

With system inertial frame velocities successfully controlled it is relatively straightforward to design a controller capable of generating $(\dot{x}_r, \dot{y}_r, \dot{\phi}_r)$ trajectories that drive the system to some arbitrary position in the inertial frame $(p_{x_r}, p_{y_r}, p_{\phi_r})$. This must be performed whilst enforcing a velocity constraint in order to bound the system's kinetic energy as to generate safe velocity trajectories. Such a controller is significant, as this allows the system to perform point-to-point translations in its environment, and is therefore a prerequisite for autonomous navigation between waypoints.

Consider the candidate Lyapunov function

$$V_\Sigma = \frac{K_p\left((p_{x_r} - x)^2 + (p_{y_r} - y)^2\right)}{2} + \frac{K_\phi\left(p_{\phi_r} - \phi\right)^2}{2} + \frac{1}{2(\overline{v}^2 - \dot{x}_r^2 - \dot{y}_r^2)} + \frac{1}{2(\overline{\dot{\phi}}^2 - \dot{\phi}_r^2)} \quad (99)$$

in which convergence of the lower velocity controller is assumed such that $\dot{x} = \dot{x}_r$, $\dot{y} = \dot{y}_r$, $\dot{\phi} = \dot{\phi}_r$. The first two terms of (99) define a cost quadratic in position error, the third term forms a barrier function enforcing the constraint $\dot{x}_r^2 + \dot{y}_r^2 < \overline{v}^2$, with a unique minimum at $\dot{x}_r = \dot{y}_r = 0$, and the last term enforces $|\dot{\phi}| < \overline{\dot{\phi}}_r$ with a unique minimum at $\dot{\phi}_r = 0$.

Substituting the control laws

$$\ddot{x}_r = -K_{v_r}\dot{x}_r + \left(\overline{v}^2 - \dot{x}_r^2 - \dot{y}_r^2\right)^2 K_p(p_{x_r} - x) \quad (100)$$

$$\ddot{y}_r = -K_{v_r}\dot{y}_r + \left(\overline{v}^2 - \dot{x}_r^2 - \dot{y}_r^2\right)^2 K_p(p_{y_r} - y) \quad (101)$$

$$\ddot{\phi}_r = -K_{\dot{\phi}}\dot{\phi}_r + (\dot{\phi}_r^2 - \overline{\dot{\phi}}_r^2)^2 K_\phi(p_{\phi_r} - \phi) \quad (102)$$

into $\dot{V}_\Sigma$ it is clear that $\dot{V}_\Sigma \leq 0 \;\forall\; \{K_{v_r}, K_{\dot{\phi}_r}\} > 0$, and that $\dot{V}_\Sigma = 0$ has a unique solution at the desired steady state, thus proving stability. Similar to the velocity controller, update of

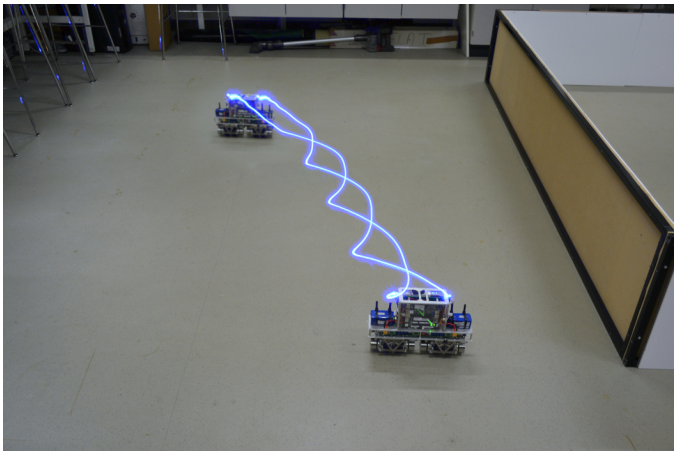

Fig. 10. A long exposure image capturing a trajectory from the origin to position references $(x_r, y_r, \phi_r) = (1, 2, 4\pi)$, in which two blue LEDs are used to capture the tracked path.

each control law is slowed by multiplication with terms of the form

$$e^{-K|\dot{x}_r - \dot{x}|}, \quad K \gg 1 \tag{103}$$

so that the assumption of lower loop convergence holds.

Fig. 11 shows the simulated response of the above controller to the reference $(p_{x_r}, p_{y_r}, p_{\phi_r}) = (2, 2, 2\pi)$, with the system initialised at the origin and with $\overline{\theta}_p = 0.6$, $\overline{v} = 1$, $\overline{v}_{xf} = 2$, and $\overline{w}_2 = 4$. $w_1 - v_x\dot{\phi}$ is shown rather than $w_1$, as this represents acceleration in the $v_x$ subsystem exclusive of that due to rotation; it is this value that is constrained by the lower velocity controller. This demonstrates asymptotic position reference tracking with minimal overshoot, and sensible smooth velocity trajectories that satisfy constraints.

Fig. 12 shows the experimental response of the prototype to exactly the same reference trajectories with identical control gains. This results in the system tracking a nearly identical position trajectory, though now there is more disturbance in the $\dot{x}$ and $\dot{y}$ states due to $\|v\|\dot{\phi} \neq 0$. Similarly, a more aggressive $\theta_p$ trajectory is required than in simulation to counter this deviation from the velocity reference. Again, all constraints are satisfied, and all state and input trajectories evolve as expected. A long exposure image demonstrating this controller is shown in Fig. 10, in which two LEDs are used to capture the resulting tracked path.

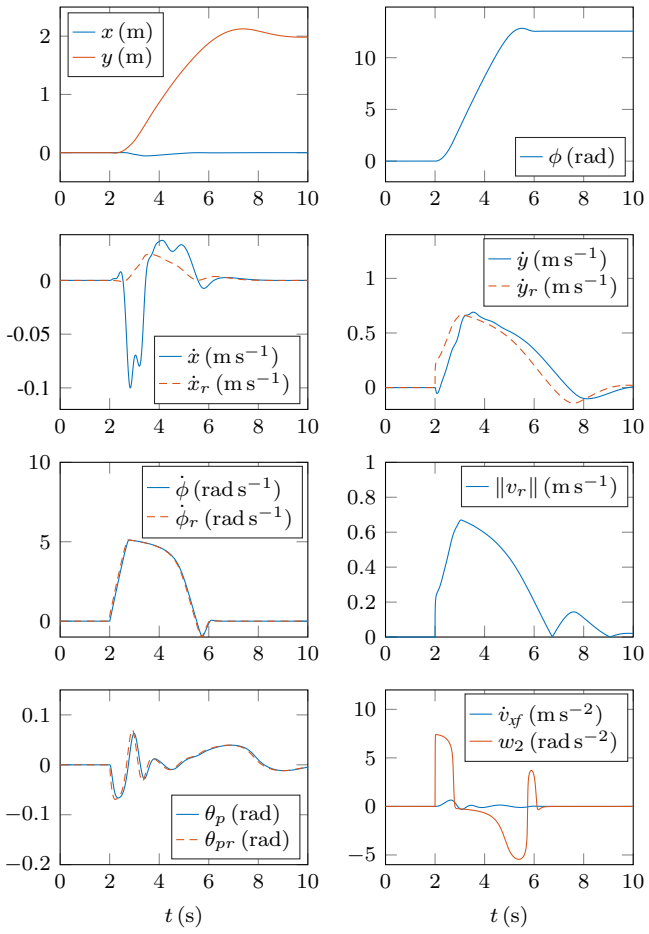


Fig. 11. Simulated system state trajectories for a reference $(x_r, y_r, \phi_r) = (2, 2, 2\pi)$, initialised at the origin with $\overline{\theta}_p = 0.6$, $\overline{v} = 1$, $\overline{v}_{xf} = 3$, and $\overline{w}_2 = 15$. $w_1 - v_x\dot{\phi}$ is shown rather than $w_1$, as this represents acceleration in the $v_x$ subsystem exclusive of that due to rotation of the body frame, and is the value that is constrained.

## VI. Conclusion

This article has derived the kinematics and dynamics models of the Collinear Mecanum Drive with linear friction models, has proven controllability, and has demonstrated a novel partial feedback linearisation, capable of transforming the CMD's dynamics from a system of six nonlinear and two linear ODEs to three nonlinear and five linear ODEs. Controllers suitable for both human-driven and autonomous applications have been derived and experimentally demonstrated, all with stability and convergence guarantees for the fully coupled nonlinear dynamics model.

The Collinear Mecanum Drive promises to yield significant improvements in manoeuvrability, grace of motion, and a step toward allowing the creation of robots with taller, slimmer form factors across a broad range of applications, ranging from personal robotics in the home and office, customer service and inventory tracking robotics in retail, and to autonomous warehousing applications.

## References

[1] U. Nagarajan, G. Kantor, and R. Hollis, "The ballbot: An omnidirectional balancing mobile robot," *The International Journal of Robotics Research*, vol. 33, no. 6, pp. 917–930, May 2014. [Online]. Available: http://journals.sagepub.com/doi/10.1177/0278364913509126

[2] M. T. Watson, D. T. Gladwin, T. J. Prescott, and S. O. Conran, "Dual-mode model predictive control of an omnidirectional wheeled inverted pendulum," *IEEE/ASME Transactions on Mechatronics*, vol. 24, no. 6, pp. 2964–2975, Dec 2019.

[3] M. T. Watson, D. T. Gladwin, T. J. Prescott, and S. O. Conran, "Velocity constrained trajectory generation for a collinear mecanum wheeled robot," in *2019 International Conference on Robotics and Automation (ICRA)*. IEEE, May 2019, pp. 4444–4450. [Online]. Available: https://ieeexplore.ieee.org/document/8794019/

[4] K. Zimmermann, I. Zeidis, and M. Abdelrahman, "Dynamics of mechanical systems with mecanum wheels," in *Springer Proceedings in Mathematics and Statistics*, vol. 93, 2014, pp. 269–279. [Online]. Available: http://doi.org/10.1007/978-3-319-08266-0_19

[5] K. M. Lynch and F. C. Park, *Modern robotics : mechanics, planning, and control*, 2017. [Online]. Available: https://books.google.co.uk/books?id=8uS3AQAACAAJ

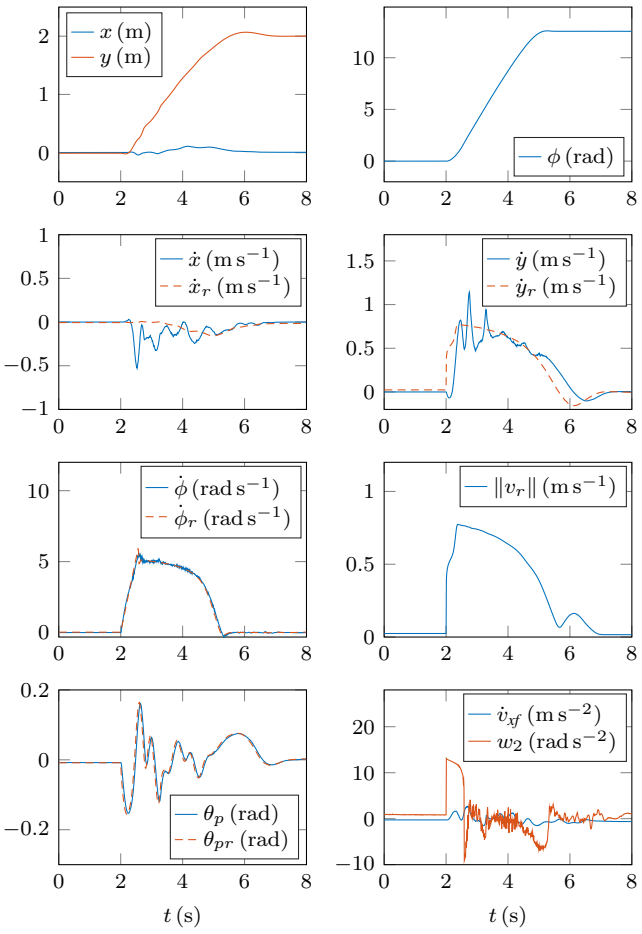


Fig. 12. Experimental system state trajectories for reference $(x_r, y_r, \phi_r) = (0, 2, 4\pi)$, initialised at the origin with $\overline{\theta}_p = 0.4$, $\overline{v} = 1$, $\overline{\dot{v}}_{xf} = 3$, $\overline{w}_2 = 15$, $\overline{v} = 1$, and $\overline{\dot{\phi}} = 6$. $w_1 - v_x\dot{\phi}$ is shown rather than $w_1$, as this represents acceleration in the $v_x$ subsystem not due to rotation, and is the value that is constrained. Small steady state errors in the tracking of $\dot{x}_r$ and $\dot{y}_r$ are due to the presence of static friction in the real-world system and a lack of integral action in the controller.


[6] H. H. Nijmeijer and A. J. van der. Schaft, *Nonlinear dynamical control systems*. Springer-Verlag, 1990. [Online]. Available: https://www.springer.com/gp/book/9780387972343

[7] A. Salerno and J. Angeles, "A new family of two-wheeled mobile robots: Modeling and controllability," *IEEE Transactions on Robotics*, vol. 23, no. 1, pp. 169–173, Feb. 2007. [Online]. Available: http://ieeexplore.ieee.org/document/4084575/

[8] B. Siciliano, L. Sciavicco, L. Villani, and O. Giuseppe, *Robotics : Modelling, Planning and Control*. Springer, 2009. [Online]. Available: https://www.springer.com/gp/book/9781846286414

[9] A. Salerno, "Design, dynamics and control of a fast two-wheeled quasiholonomic robot," Ph.D. dissertation, McGill University, 2006. [Online]. Available: https://core.ac.uk/download/pdf/41887250.pdf

[10] K. Pathak, J. Franch, and S. K. Agrawal, "Velocity and position control of a wheeled inverted pendulum by partial feedback linearization," *IEEE Transactions on Robotics*, vol. 21, no. 3, pp. 505–513, Jun. 2005. [Online]. Available: http://ieeexplore.ieee.org/document/1435497/

[11] R. Marino, "On the largest feedback linearizable subsystem," *Systems and Control Letters*, vol. 6, no. 5, pp. 345–351, Jan. 1986. [Online]. Available: https://doi.org/10.1016/0167-6911(86)90130-1

[12] A. J. Fossard and D. Normand-Cyrot, *Nonlinear Systems : Control 3*. Springer US, 1997. [Online]. Available: https://doi.org/10.1007/978-1-4615-6395-2

[13] A. Isidori, *Nonlinear Control Systems*, ser. Communications and Control Engineering. London: Springer London, 1995. [Online]. Available: http://link.springer.com/10.1007/978-1-84628-615-5

[14] B. Srinivasan, P. Huguenin, and D. Bonvin, "Global stabilization of an inverted pendulum: Control strategy and experimental verification," *Automatica*, vol. 45, no. 1, pp. 265–269, Jan. 2009. [Online]. Available: https://doi.org/10.1016/j.automatica.2008.07.004

[15] Wei Zhong and H. Rock, "Energy and passivity based control of the double inverted pendulum on a cart," in *Proceedings of the 2001 IEEE International Conference on Control Applications (CCA'01) (Cat. No.01CH37204)*. IEEE, 2002, pp. 896–901. [Online]. Available: http://ieeexplore.ieee.org/document/973983/

[16] M. W. Spong, P. Corke, and R. Lozano, "Nonlinear control of the reaction wheel pendulum," *Automatica*, vol. 37, no. 11, pp. 1845–1851, Nov. 2001. [Online]. Available: https://doi.org/10.1016/S0005-1098(01)00145-5

[17] M. W. Spong, "The swing up control problem for the acrobot," *IEEE Control Systems*, vol. 15, no. 1, pp. 49–55, Feb. 1995. [Online]. Available: https://ieeexplore.ieee.org/document/341864/

[18] J. Hauser and R. M. Murray, "Nonlinear controllers for non-integrable systems: the acrobot example," in *1990 American Control Conference*. IEEE, May 1990, pp. 669–671. [Online]. Available: https://ieeexplore.ieee.org/document/4790817/

[19] M. A. Karkoub and M. Parent, "Modelling and non-linear feedback stabilization of a two-wheel vehicle," *Proceedings of the Institution of Mechanical Engineers, Part I: Journal of Systems and Control Engineering*, vol. 218, no. 8, pp. 675–686, Dec. 2004. [Online]. Available: http://journals.sagepub.com/doi/10.1177/095965180421800807

[20] R. M. Brisilla and V. Sankaranarayanan, "Nonlinear control of mobile inverted pendulum," *Robotics and Autonomous Systems*, vol. 70, pp. 145–155, 2015. [Online]. Available: http://dx.doi.org/10.1016/j.robot.2015.02.012

[21] H. K. Khalil, *Nonlinear Systems*. Prentice Hall, 1996, vol. 3.

[22] K. P. Tee, S. S. Ge, and E. H. Tay, "Barrier Lyapunov functions for the control of output-constrained nonlinear systems," *Automatica*, vol. 45, no. 4, pp. 918–927, 2009. [Online]. Available: https://doi.org/10.1016/j.automatica.2008.11.017


**Matthew T. Watson** received the M.Eng. (Hons.) degree in electronic engineering from the University of Sheffield, U.K. in 2014. In 2019 he successfully defended his PhD thesis 'The Collinear Mecanum Drive', written during his time as a researcher in the Department of Electronic and Electrical Engineering at the University of Sheffield. His current research concerns the modelling and control of novel autonomous systems, real time trajectory optimisation for complex dynamic systems, and novel approaches to the control of micro aerial vehicles in dynamic and unstructured environments.

**Daniel T. Gladwin** received the M.Eng. (Hons.) degree in electronic engineering (computer architecture) and the Ph.D. degree in automated control structure design and optimization using evolutionary computing from the University of Sheffield, Sheffield, UK, in 2004 and 2009, respectively. In 2012, he was appointed a Lecturer at the University of Sheffield and became Senior Lecturer in 2017 and Professor in 2020. He is a founding member and Deputy Director of the Centre for Research into Electrical Energy Storage and Applications (CREESA) at the University of Sheffield. His current research interests include robotics, energy storage and management, optimization, and intelligent systems.

**Tony J. Prescott** holds an MA degree in Psychology from the University of Edinburgh, U.K., an MSc degree in Applied Artificial Intelligence from the University of Aberdeen, U.K., and a PhD in Machine Learning from the University of Sheffield, UK. He is a currently a Professor of Cognitive Robotics in the Department of Computer Science at the University of Sheffield. He is also a co-founder and the current Director of *Sheffield Robotics* a cross-disciplinary institute across both universities in Sheffield. He has authored over 200 publications in robotics, computational modeling, cognitive science and computational neuroscience.